AD NUMBER

ADB016599

LIMITATION CHANGES

TO:

Approved for public release; distribution is unlimited.

FROM:

Distribution authorized to U.S. Gov't. agencies only; Test and Evaluation; NOV 1976. Other requests shall be referred to Air Force Weapons Lab., Kirtland AFB, NM.

AUTHORITY

AFWL ltr 7 Nov 1986

AD B016599

AUTHORITY:
AFWL etc.,
7 NOV 86

AFWL-TR-76-124

AFWL-TR-
76-124

RESISTOR SUSCEPTIBILITY SURVEY

Boeing Aerospace Company
Seattle, Washington 98124

BDM Corporation
Albuquerque, NM 87108

November 1976

Final Report

This research was sponsored by the Defense Nuclear Agency under Subtask R99QAXEB0971, Work Unit 32, Subtask Title: Theoretical and Experimental EMP Vulnerability.

Prepared for
Director
DEFENSE NUCLEAR AGENCY
Washington, DC 20305

AIR FORCE WEAPONS LABORATORY
Air Force Systems Command
Kirtland Air Force Base, NM 87117

AFWL-TR-76-124

This final report was prepared by the Boeing Aerospace Company, Seattle, Washington and the BDM Corporation, Albuquerque, New Mexico, under Contract F29601-72-C-0028, Job Order WDNE1403 with the Air Force Weapons Laboratory, Kirtland Air Force Base, New Mexico. Lt Joel W. Robertson (DYX) was the Laboratory Project Officer-in-Charge.

When US Government drawings, specifications, or other data are used for any purpose other than a definitely related Government procurement operation, the Government thereby incurs no responsibility nor any obligation whatsoever, and the fact that the Government may have formulated, furnished, or in any way supplied the said drawings, specifications, or other data is not to be regarded by implication or otherwise as in any manner licensing the holder or any other person or corporation or conveying any rights or permission to manufacture, use, or sell any patented invention that may in any way be related thereto.

This technical report has been reviewed and is approved for publication.

Joel W. Robertson
JOEL W. ROBERTSON
Lt, USAF
Project Officer

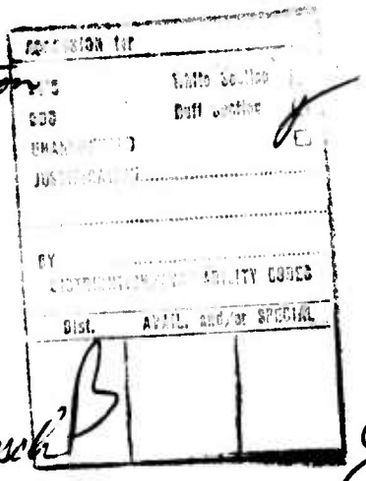

FOR THE COMMANDER

Donald C. Wunsch
DONALD C. WUNSCH
Acting Chief, Applied Research Branch

John S. DeWitt
JOHN S. DeWITT
Lt Colonel, USAF
Chief, Technology Division

DO NOT RETURN THIS COPY. RETAIN OR DESTROY.

UNCLASSIFIED

SECURITY CLASSIFICATION OF THIS PAGE (When Data Entered)

REPORT DOCUMENTATION PAGE

READ INSTRUCTIONS BEFORE COMPLETING FORM

1. REPORT NUMBER: AFWL-TR-76-124	2. GOVT ACCESSION NO.
3. RECIPIENT'S CATALOG NUMBER	
4. TITLE (and Subtitle): RESISTOR SUSCEPTIBILITY SURVEY	5. TYPE OF REPORT & PERIOD COVERED: Final Report
6. PERFORMING ORG. REPORT NUMBER: BDM/A-75-10-TR	
7. AUTHOR(s): C. G. Hoover, K. S. Kunz, T. H. Lehman, R. N. Randall, G. J. Rimbert, J. J. Schwarz	8. CONTRACT OR GRANT NUMBER(s): F29601-72-C-0028 Work Order 2-14
9. PERFORMING ORGANIZATION NAME AND ADDRESS: Boeing Aerospace Company, Seattle, WA 98124 BDM Corporation, Albuquerque, NM 87108	10. PROGRAM ELEMENT, PROJECT, TASK AREA & WORK UNIT NUMBERS: 62704H WDNE 1403
11. CONTROLLING OFFICE NAME AND ADDRESS: Air Force Weapons Laboratory (DYX) Kirtland Air Force Base, New Mexico 87117	12. REPORT DATE: Nov 1976
	13. NUMBER OF PAGES: 74
14. MONITORING AGENCY NAME & ADDRESS (if different from Controlling Office): Director Defense Nuclear Agency Washington, D.C. 20305	15. SECURITY CLASS. (of this report): UNCLASSIFIED
	15a. DECLASSIFICATION/DOWNGRADING SCHEDULE

16. DISTRIBUTION STATEMENT (of this Report)

Distribution limited to US Government agencies only because test and evaluation of military systems (Nov 76). Other requests for this document must be referred to AFWL (DYX), Kirtland Air Force Base, New Mexico 87117.

17. DISTRIBUTION STATEMENT (of the abstract entered in Block 20, if different from Report)

18. SUPPLEMENTARY NOTES

This research sponsored by the Defense Nuclear Agency under Subtask R99QAXEB097132, Subtask Title: Theoretical and Experimental EMP Vulnerability.

19. KEY WORDS (Continue on reverse side if necessary and identify by block number)

Damage Test
Electromagnetic Pulse
Resistor Model

20. ABSTRACT (Continue on reverse side if necessary and identify by block number)

This report describes a program to survey the susceptibility of resistors to damage caused by the electrical transients associated with EMP. The program included an experimental effort to determine failure thresholds for a selection of resistors and a theoretical analysis to develop failure models.

DD FORM 1 JAN 73 1473 EDITION OF 1 NOV 65 IS OBSOLETE

UNCLASSIFIED

SECURITY CLASSIFICATION OF THIS PAGE (When Data Entered)

059610

PREFACE

This report describes a program to survey the susceptibility of resistors to damage caused by the electrical transients associated with EMP. The program included an experimental effort to determine failure thresholds for a selection of resistors and a theoretical analysis to develop failure models. The resistor test program consisted of injecting selected resistor types with electrical transients whose amplitude was increased until failure occurred. Data were obtained for a number of pulse widths where failure was defined as a change in resistance beyond the normal tolerance. Tests were performed on a total of 13 resistor types obtained from 6 manufacturers. The theoretical effort consisted of developing a thermal failure model for a metal film resistor. Good correlation was observed between empirical and theoretical results.

This report was prepared by The BDM Corporation, Albuquerque, New Mexico under subcontract to The Boeing Aerospace Company, Seattle, Washington, Work Order 2-14 of Contract F29601-72-C-0028 for the Air Force Weapons Laboratory, Kirtland Air Force Base, New Mexico. The AFWL Project Officer was Lt Joel W. Robertson. The former Project Officer was Captain G. Michaelidis. The Task Officer was D. C. Wunsch. The Boeing Program Manager was J. J. Dicomes and the principal investigator for this work order is B. P. Gage. The BDM effort was directed by J. J. Schwarz. Technical contributors to this effort were: C. G. Hoover, K. S. Kunz, T. H. Lehman, R. N. Randall, and G. J. Rimbert.

This project was supported by the Defense Nuclear Agency under subtask R990AXEB097, work unit 42. The Project Officers at DNA were Major D. R. Carlson and Major W. Dean.

TABLE OF CONTENTS

SECTION		PAGE
I	INTRODUCTION	5
	1. GENERAL	5
	2. TEST PROGRAM SUMMARY	5
	3. SUMMARY OF THEORETICAL RESULTS	11
II	PULSE TEST IMPLEMENTATION	13
	1. RESISTOR SELECTION	13
	2. PULSE TESTING	14
	3. DATA REDUCTION	18
III	TEST RESULTS	21
	1. RESISTOR FAILURE MODES	21
	2. FAILURE POWER VERSUS RESISTOR CONSTRUCTION	23
	3. FAILURE POWER VERSUS RATED POWER DISSIPATION	26
	4. FAILURE POWER VERSUS RESISTANCE	27
	5. FAILURE POWER VERSUS MANUFACTURER	27
	6. ARCING TESTS	30
	7. DATA SUMMARY	32
IV	RESISTOR MODELING	34
	1. GENERAL	34
	2. THERMAL MODEL CONSIDERATIONS	35
	3. HOMOGENEOUS MODEL	39
	4. COMPOSITE MODEL	41
V	DISCUSSION OF RESULTS	51
	APPENDICES	
A	MATERIAL SPECIFICATIONS	57

LIST OF ILLUSTRATIONS

Figure		Page
1	Failure Power Dependence on Construction for 1/8 W, 50 Ω Resistors	7
2	Comparison of Component Failure Power	8
3	Component Comparison	10
4	Model Comparison	12
5	Resistor Pulse Test Equipment	16
6	Resistor Test Station/Velonex 350 Pulser	17
7	Resistor Test Station/BDM SN/SPG-200 Pulser	19
8	Typical Digitized Waveforms	20
9	Failure Power Versus Pulse Width for 50 Ω Resistors	22
10	Failure Power Dependence on Construction for 1/8 W, 50 Ω Resistors	25
11	Failure Power Plate for Metal Oxide Resistor	28
12	Failure Power Dependence on Resistance for Metal Film Resistors	29
13	Cross Section of Infinite Composite Cylinder	42
14	Model Comparison	52
15	Model Comparison	56
A-1	Electric Resistivity -- Nickel + Chromium	58
A-2	Specific Heat -- Nickel + Chromium + X	59
A-3	Thermal Conductivity -- Nickel + Chromium + X	60
A-4	Specific Heat -- Aluminum Oxide	61
A-5	Thermal Conductivity -- Aluminum Oxide	62

SECTION I

INTRODUCTION

1. GENERAL

This report describes a program to survey the susceptibility of resistors to damage caused by the electrical transients associated with the electromagnetic pulse (EMP). The program included an experimental effort to determine failure thresholds for a selection of resistors and a theoretical analysis to develop failure models.

The susceptibility of electronic subsystems to EMP induced damage has been historically tied to the susceptibility of junction semiconductor devices. The impact of nonsemiconductor devices on circuit susceptibility has not been investigated in detail, even though the limited data available has indicated that some types of resistors and capacitors exhibit failure thresholds similar to semiconductor devices. Since they comprise a substantial portion of the electronic components in a military system, it is important to obtain data to describe the failure characteristics of nonsemiconductor devices. The effort described here constitutes a first step in the study of resistors.

2. TEST PROGRAM SUMMARY

The resistor test program consisted of injecting selected resistor types with electrical transients whose amplitude was increased until failure occurred. Data was obtained for a number of pulse widths. The resistance was measured before and after each pulse and failure was defined as a change in resistance beyond the normal tolerance. Tests were performed on a total of 13 resistor types obtained from 6 manufacturers. Since the program goal was a resistor survey, the sample size was limited.

The primary program goal of performing a survey of the available low power resistors was accomplished. Five different resistor construction techniques were evaluated. Their relative hardness can be judged from the following data for 1/8 watt 50 ohm resistors subjected to 1 μs and 100 μs pulses.

CONSTRUCTION	VENDOR	NUMBER	POWER (WATTS) 1 μs	100 μs
Metal Film	Dale	RN55D	6800	600
Metal Film	TRW	RN55C	-	1600
Metal Oxide	Corning	C-4	39500	550
Carbon Comp	Allan Bradley	RCR05G	294,000*	9500
Wire Wound	RCL	7009ER	206,000*	29700*

*No Fail

The entry for the wire wound resistor is the maximum no-fail power since the available pulsers were unable to fail any wire wound resistors. Generally speaking, the relative hardness can be seen from the entries in the 100 μs column. However, the 100 μs pulse width is rather large to evaluate relative hardness for EMP transients. This is better accomplished at 1 μs. Using the latter data, it can clearly be seen that the Dale metal film resistor is the softest category for the pulse widths of primary interest for EMP. This comparison is also shown in Figure 1 which plots failure power versus pulse width for the metal film and metal oxide resistors.

As seen in Figure 1, the resistor failure power was found to vary with the pulse width. The general trend was similar to that observed previously for semiconductor devices. Figure 2 provides a comparison of the RN55D resistor to a 2N2222 transistor. It is seen that the failure thresholds are comparable and also that the general power time relationship is similar. This observation tends to indicate that a thermal failure mechanism similar to that previously developed for semiconductor devices could also be applied to metal film resistors.

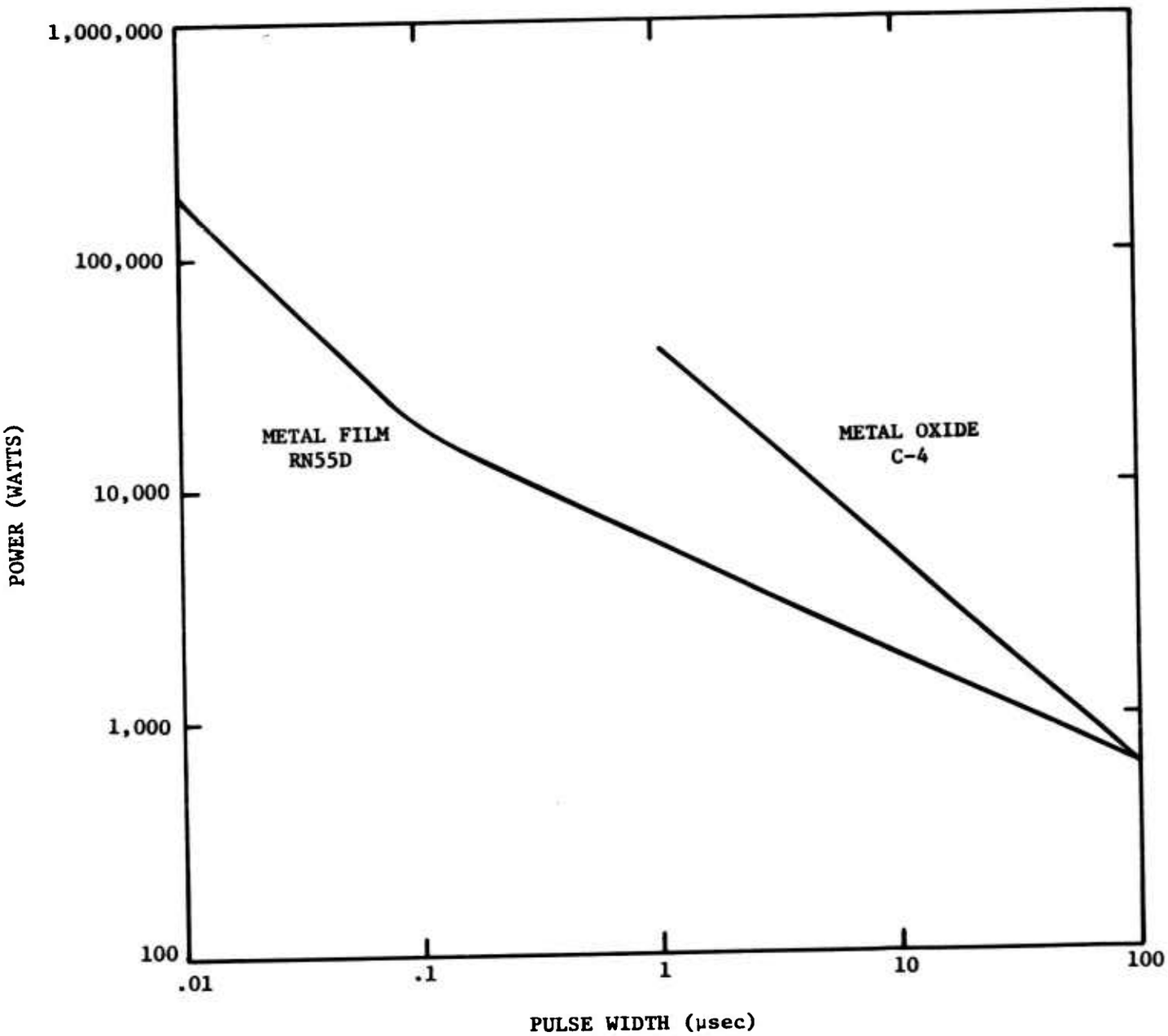

Figure 1. Failure Power Dependence on Construction for 1/8 W, 50 Ω Resistors

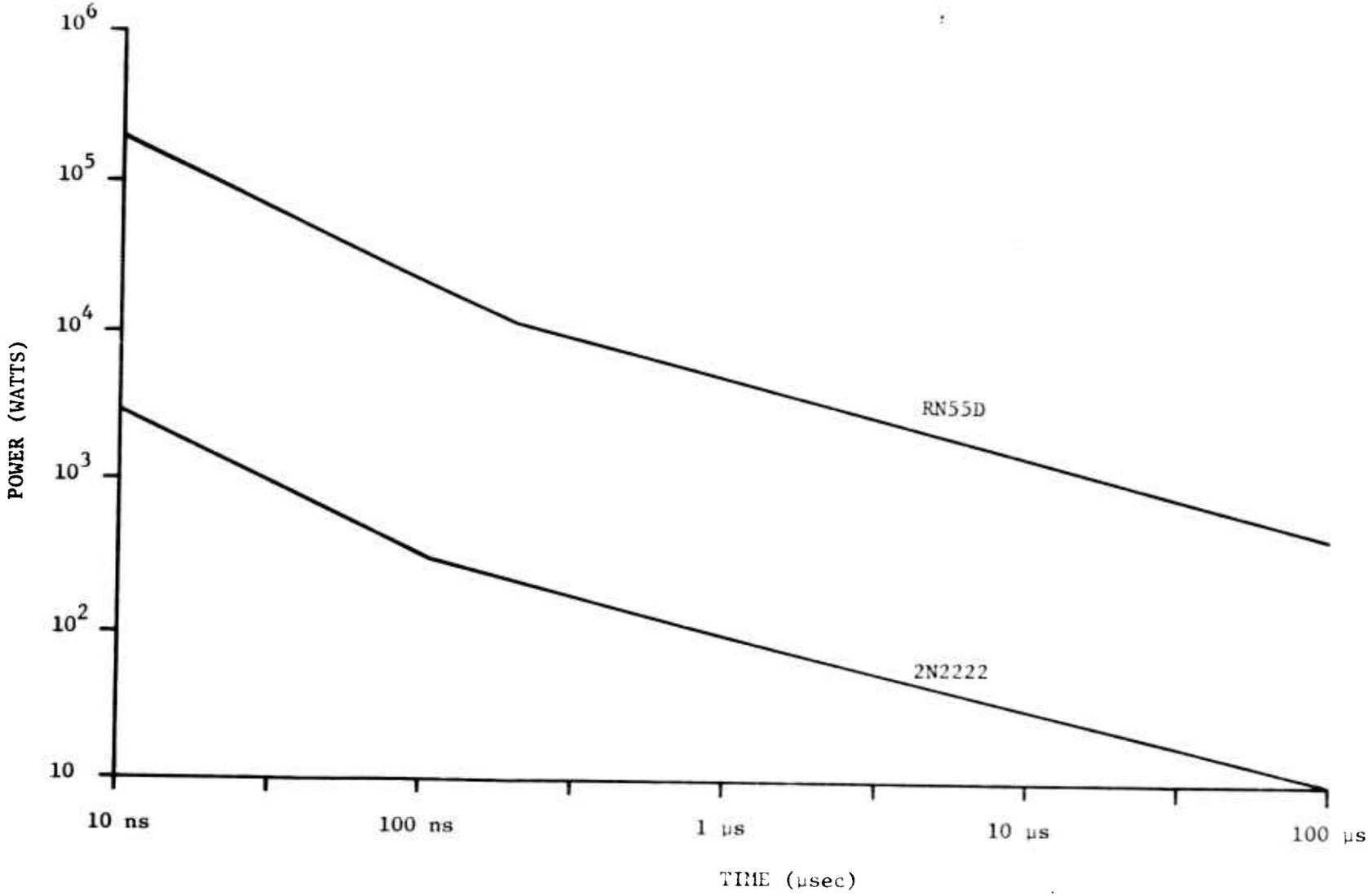

Figure 2. Comparison of Component Failure Power

2

Figure 3 is a histogram showing the distribution of the damage constant obtained experimentally for transistors and diodes. The damage constant is an average fit to the equation $P = Kt^{-1/2}$. Figure 3 also contains an equivalent damage constant K for the five resistor construction types evaluated on this program. It can be seen from the general shape of the histogram that for the test sample, resistors are generally harder than transistors and diodes. However, the softer resistors are comparable to the transistors and diodes of moderate hardness. From the test results, it appears that carbon composition and wire wound resistors are generally much harder than the other resistor types and are probably not susceptible to most EMP transients.

While the primary goal of the program was to survey a range of resistors, examination of the test data leads to a number of empirical observations concerning trends within the resistor sample. These trends are summarized here and discussed in more detail in Section III. First, there appears to be a strong relationship between failure power and rated dissipation power. For most of the resistors observed failure power was nearly proportional to rated power dissipation. Second, although there is considerable variation in observed hardness for a given resistor type there appears to be little variation which can be directly attributable to manufacturer differences. Finally, there is no consistent relationship between failure power and resistance. The tendancy is for failure power to decrease with increasing resistance. However, the actual relationship is quite complex.

An additional series of tests were performed to determine the arcing characteristics of a few resistor types. It was found that the metal film, metal oxide, and carbon composition resistors failed due to excessive power before they arced. The higher resistor values were observed to withstand voltages in excess of 10 kV without arcing. A special case was a carbon film resistor which exhibited arcing internally at a very repeatable 3 kV. This was found to be attributable to the unique construction characteristics of the resistor, wherein the leads acted like a spark gap within the body.

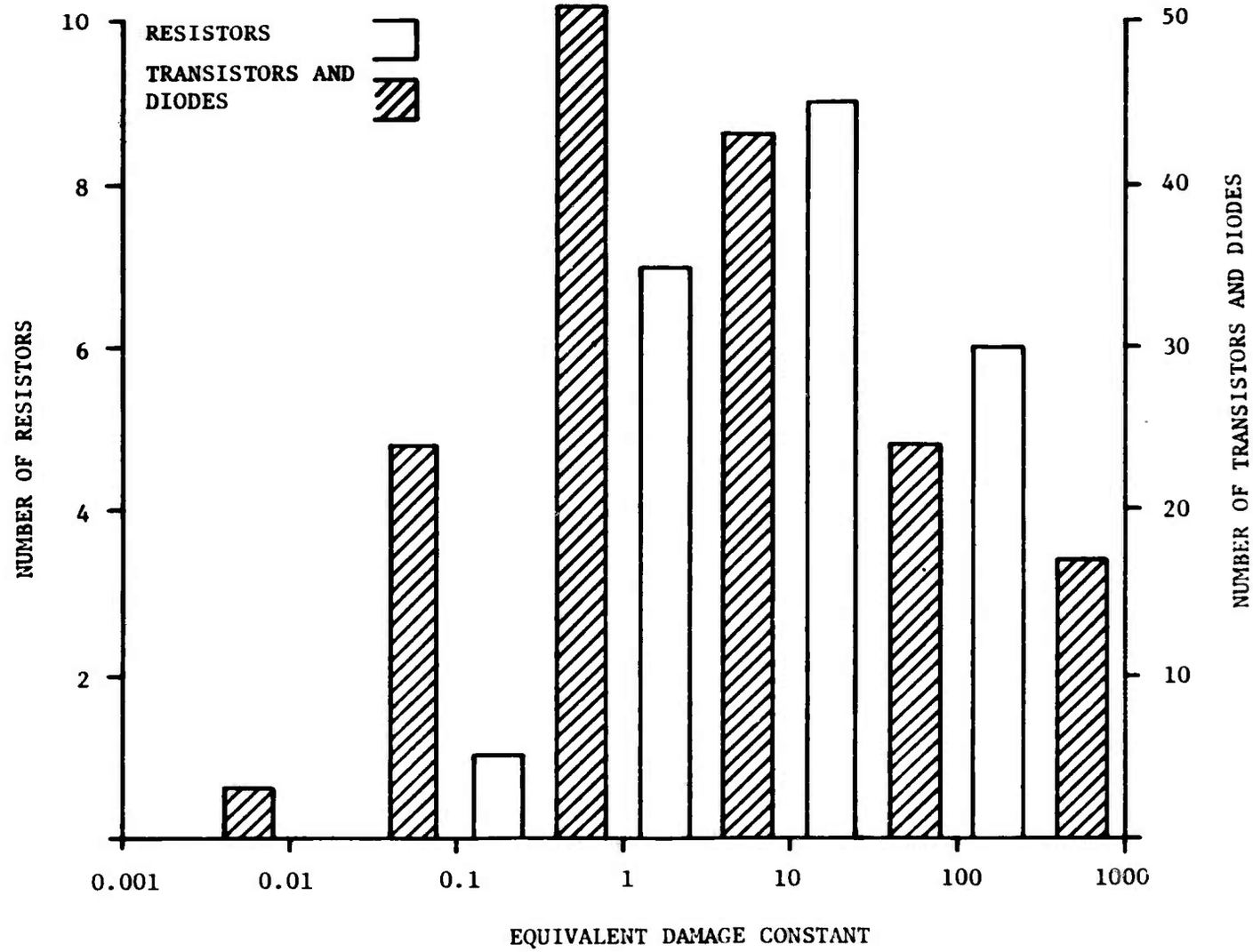

Figure 3. Component Comparison

3. SUMMARY OF THEORETICAL RESULTS

A thermal failure model was developed for a metal film resistor. The model was derived from the heat transfer equation of motion with appropriate boundary conditions and simplifying assumptions. Actually, two models were developed. The first model describes a homogeneous isotropic block of resistive material with uniform heating. The second models describes an infinite composite cylinder comprised of a continuous cylindrical shell of resistive material in intimate contact with a cylindrical rod of substrate. The composite model was shown to provide a good approximation to the observed failure data. The form of the model is

$$P = \frac{a}{e^{b^2} \operatorname{erfc} b - 1 + 2b/\sqrt{\pi}}$$

The model can be conveniently expressed as two equations dealing with different time regimes. For an RN55D resistor with a film thickness of 1000 Å, the equations are

$$P = 130t^{-1/2} \text{ Watts} \qquad \text{for } t > 25 \text{ ns}$$

$$P = 6.5 \times 10^{-3} t^{-1} \text{ Watts} \qquad \text{for } t < 1 \text{ ns.}$$

While it is possible to use the single expression for the entire time history, it is simpler to use these equations and to interpolate for the intervening pulse widths.

The composite model is compared to the measured data for the RN55D in Figure 4. The model is evaluated for two film thicknesses and experimental data is provided for changes in resistance of both 10% and 100%. The agreement between theory and experiment is seen to be very good and it is concluded that the thermal model is an appropriate choice for a metal film resistor.

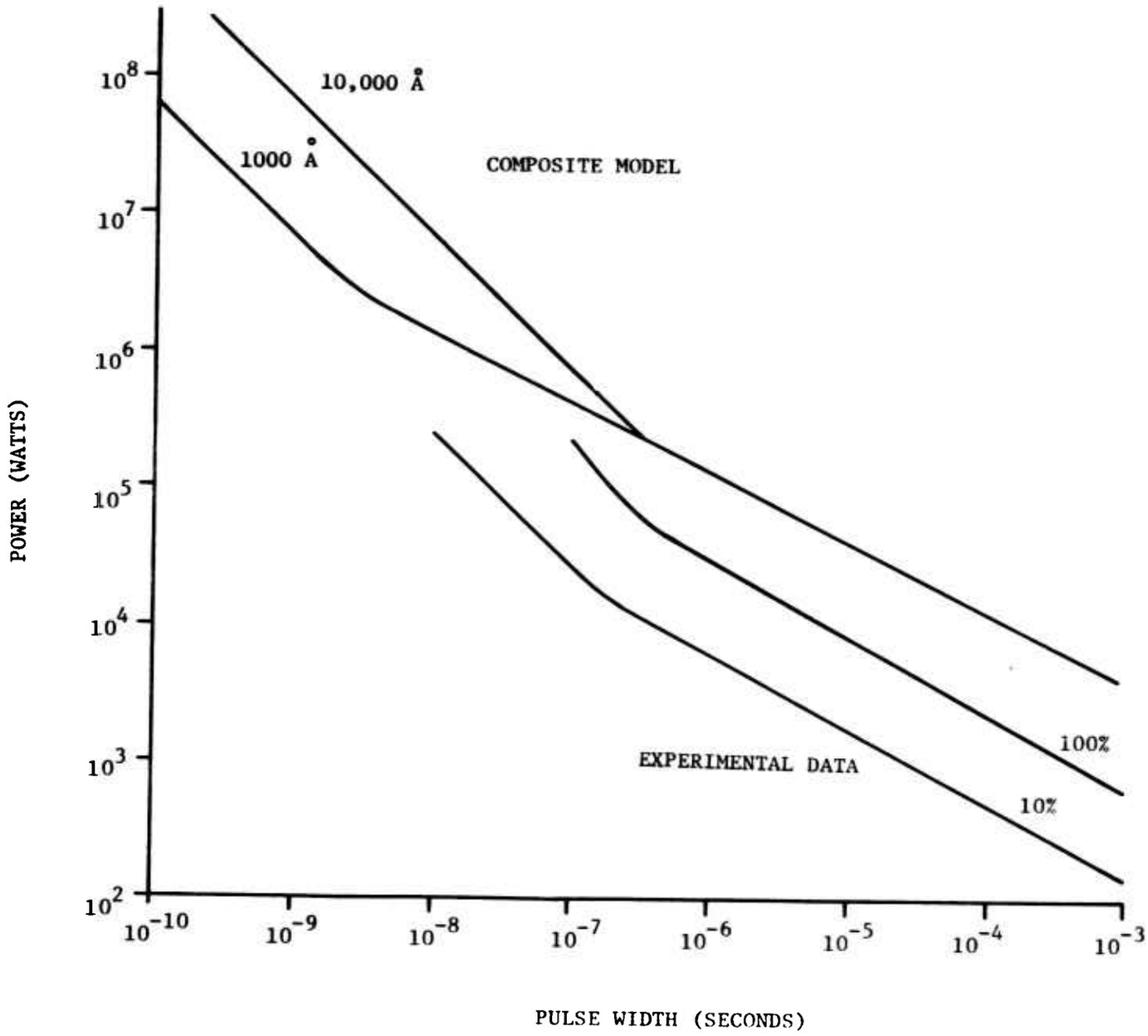

Figure 4. Model Comparison

SECTION II

PULSE TEST IMPLEMENTATION

1. RESISTOR SELECTION

This section briefly describes the implementation of the resistor test program. The description includes resistor selection, pulse testing, and data reduction.

The resistor selection involved examining the resistor market to define the required test sample. Approximately 40 resistor manufacturers were contacted for information. Of these, 20 manufacturers responded by providing descriptive information. The literature was catalogued and reviewed and as a result, five resistor construction types were defined for survey testing. The five types are

(1) Metal Film
(2) Metal Oxide
(3) Carbon Film
(4) Carbon Composition
(5) Wire Wound.

A representative sample was ordered from each construction type from a total of six manufacturers. The sample included dissipation power ratings from 1/10 watt to 2 watts. The resistor values were selected to match the source impedance of the Velonex Pulse Generator. The values are: 3 Ω, 12.4 Ω, 50 Ω, 200 Ω, 806 Ω, 3.24 kΩ, 13 kΩ and 30 kΩ.

The test sample was selected to complete a comprehensive resistor survey. Unfortunately, the delay times associated with resistor delivery

were so long that a substantial portion of the sample arrived too late to be included in the test. Of the resistors obtained, the largest values were generally delivered first and these were the hardest to fail. As a result, a number of otherwise desirable tests were not performed. Table 1 shows the resistors tested and defines the construction, manufacturer, and number. In most cases, each entry corresponds to tests of multiple resistance values and multiple pulse widths.

2. PULSE TESTING

As each resistor was received, it was tagged with a unique serial number for future identification. Then, a pretest resistance characterization was performed to determine the initial conditions of the test sample. The resistance measurements were made on a digital ohm-meter.

A block diagram of the resistor pulse test equipment is shown in Figure 5 and a photograph is shown in Figure 6. The resistor under test is inserted in a special test fixture which provides access for the voltage and current probes. The pulse environment is provided by a Velonex type 360 pulse generator with plug-ins chosen to achieve the maximum power transfer to the test resistor. Voltage and current are recorded on a Tektronix type 555 dual beam oscilloscope with a C27 camera. This allows both parameters to be displayed on the same photograph which eases later data reduction.

A major problem was the low power output of the Velonex Pulse Generator. Plug-ins must be selected for both their source impedance and their pulse width capability. As a result, it was often found that the resistors could not be failed at all, or could only be failed at one or two pulse widths. To alleviate this problem the BDM SN/SPG-200 Pulse Generator was used in a few instances where high power short duration pulses were required. In this case, a T&M Research voltage probe and current viewing

Table 1. Resistor Types Tested

CONSTRUCTION	NUMBER	MANUFACTURER
METAL FILM	RN55	DALE, TRW
	RN60	TRW
	RN65	DALE, TRW, T.I.
	RN70	DALE
CARBON FILM	MC 1/10	DALE
	MC 1/4	DALE
METAL OXIDE	C3	CORNING
	C4	CORNING
	C5	CORNING
CARBON COMPOSITION	RCR05	ALLEN BRADLEY
	RCR07	TRW
WIRE WOUND	7009	RCL
	WWA-24	DALE

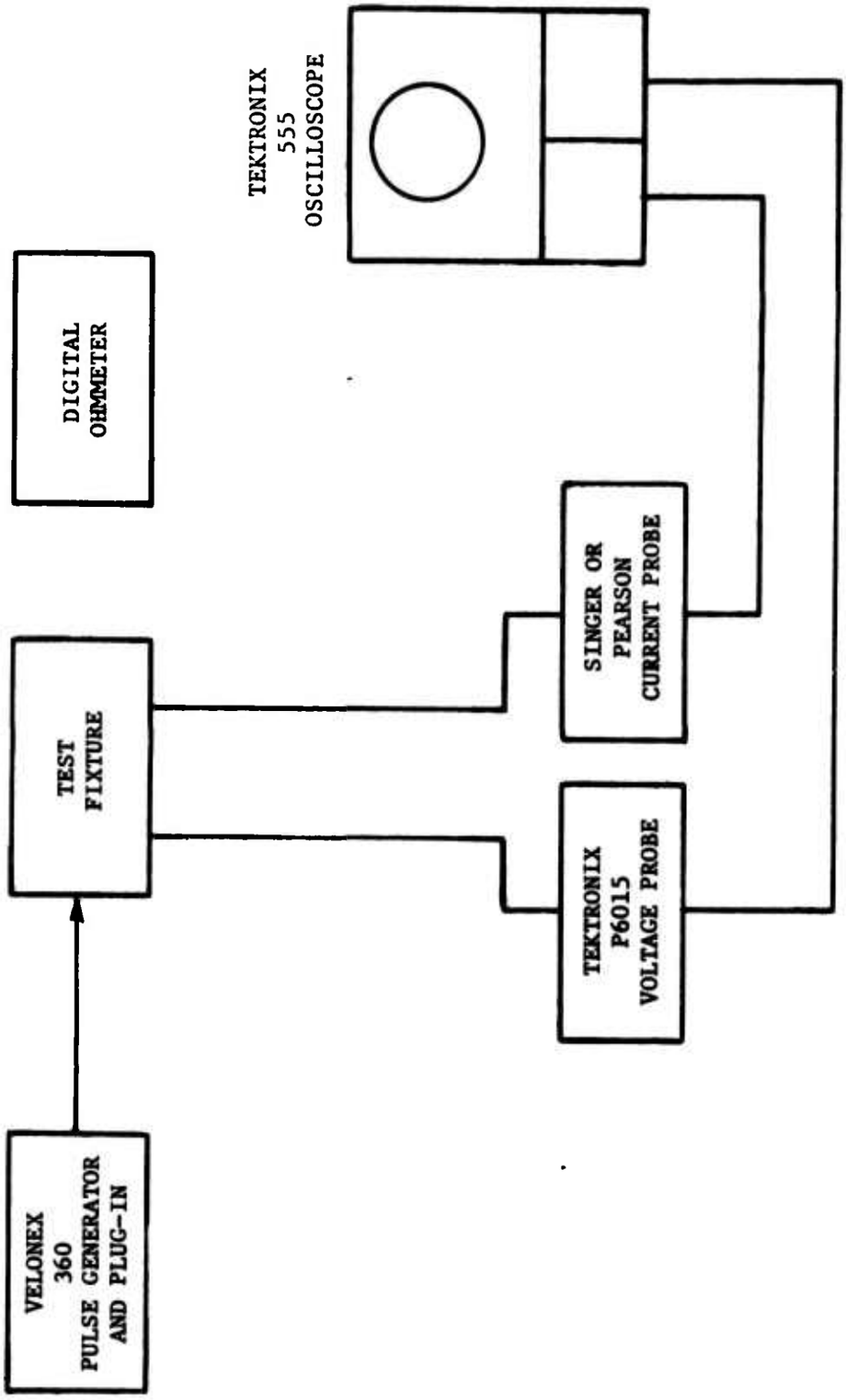

Figure 5. Resistor Pulse Test Equipment

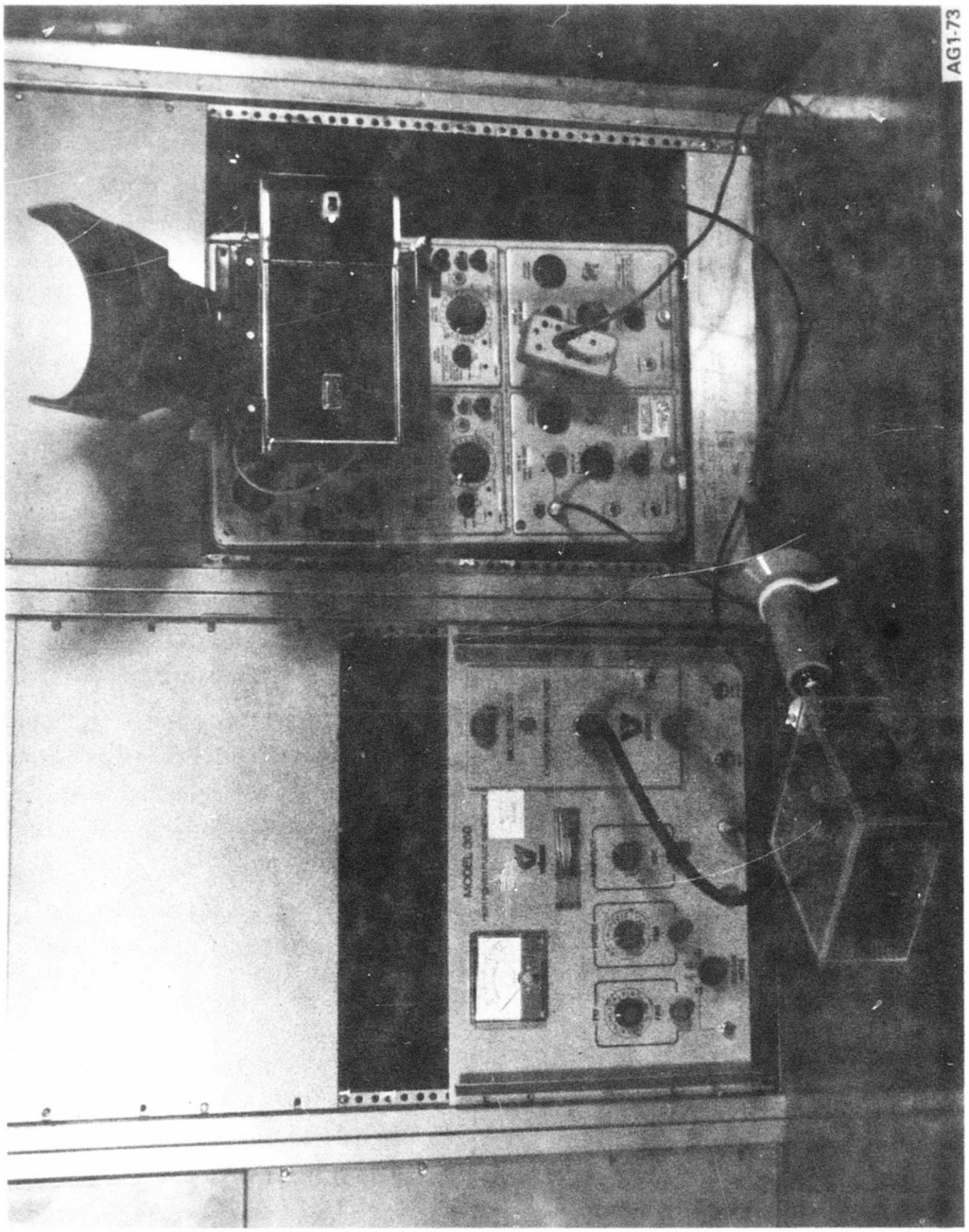

Figure 6. Resistor Test Station/Velonex 350 Pulser

resistor were used and the data was recorded on a Tektronix 7912 oscilloscope. This configuration is shown in Figure 7.

The general test procedure was to obtain data at up to four pulse widths. These are 0.1 μs, 1 μs, 10 μs, and 100 μs. Each resistor test began with a minimum pulse level followed by a resistance measurement. If the resistance change was less than 10%, the pulse generator output was incremented and the test repeated. This procedure was iterated until the device failed.

3. DATA REDUCTION

The data reduction consisted of processing Polaroid oscilloscope photos to obtain plots of failure power versus pulse width. The primary data reduction was accomplished by digitizing the voltage and current waveforms using a Hewlett Packard model 9820 calculator system with digitizer and plotter. In some cases, due to the work load of the 9820 system, traces were reduced manually.

The matched current and voltage waveform pairs were digitized and the calculator was programmed to compute instantaneous power and total energy versus time. Figure 8 shows a typical plot of these digitization/calculation results including voltage (V), current (I), Power (P), and Energy (E). The average power is determined by dividing the energy at failure by the time to failure. Log-log plots of the average power versus time are then made.

All resistor test data including Polaroid photographs, digitized plots, power versus time plots, and data summaries were catalogued and filed for later access in 3-ring loose leaf binders. Copies of the data summaries and the plots were made to facilitate access to the information.

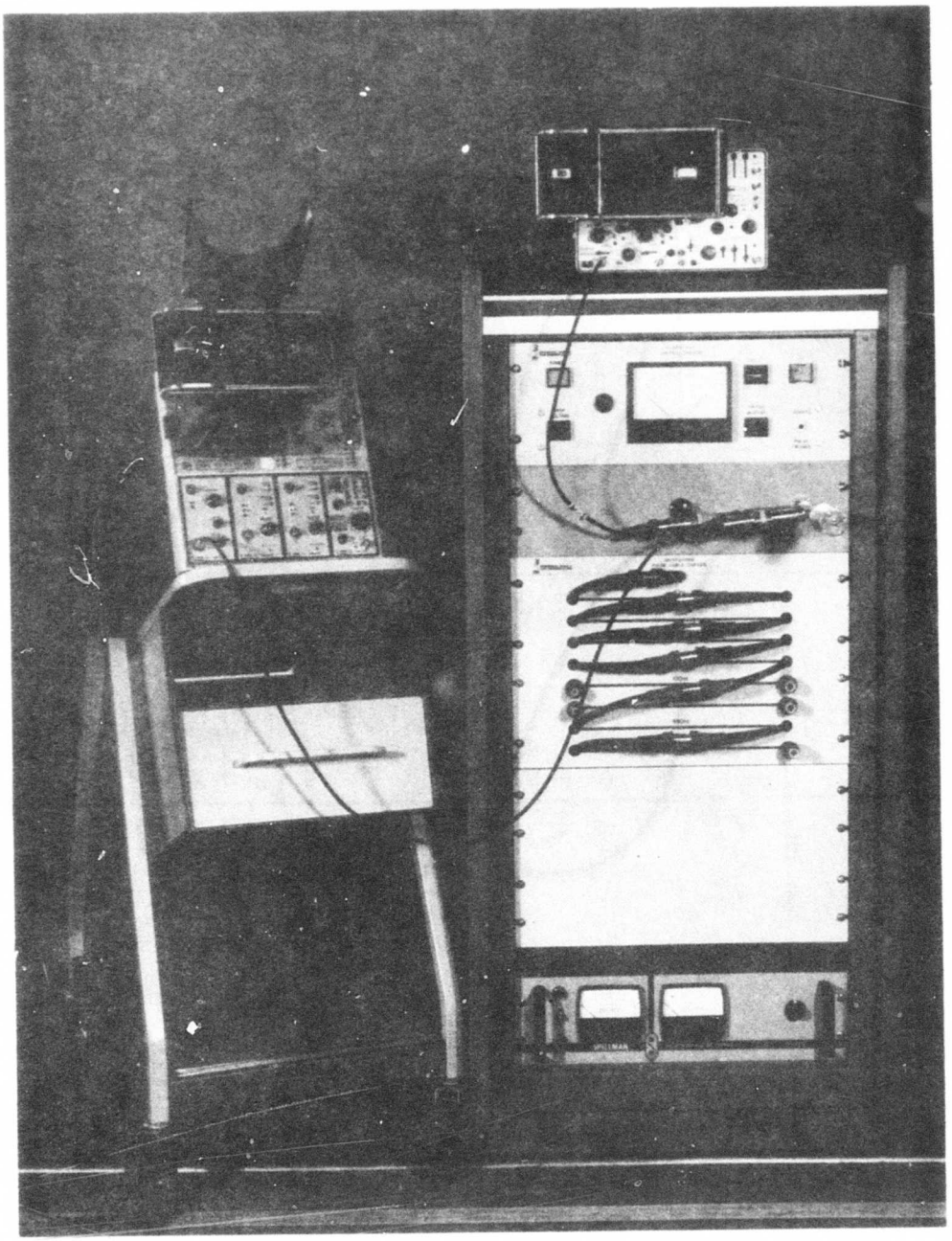

Figure 7. Resistor Test Station/BDM SN/SPG-200 Pulser

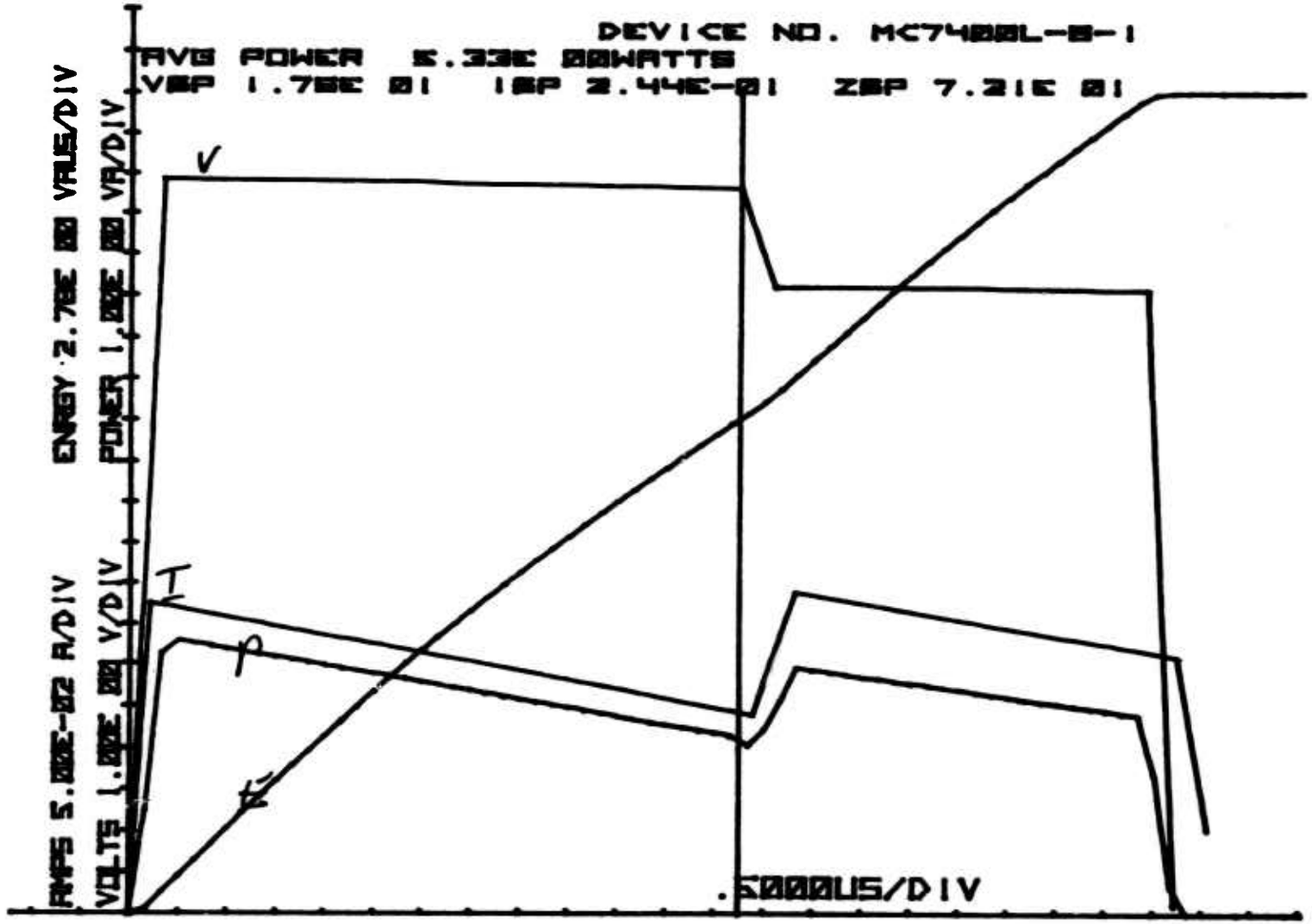

Figure 8. Typical Digitized Waveforms

SECTION III

TEST RESULTS

1. RESISTOR FAILURE MODES

The primary goal of the program was to perform an empirical survey to rate the five resistor construction types for relative hardness to electrical transients. In addition, data was obtained to allow preliminary determination of the variation of failure power as a function of other resistor parameters. These include: rated dissipation power, resistance, and manufacturer.

As indicated in Section I, the general failure characteristics of the resistors tested seem to be similar to the failure characteristics of transistors and diodes tested previously. Since it was not possible to perform microscopic examinations of the resistors, the failure mode could not be observed directly. However, the apparent similarity to the transistor and diode failure characteristics indicates that the probable failure mode is thermal. As such, the shape of the failure power versus pulse width curve is determined by a number of characteristics including the thermal time constant. Figure 9 shows failure curves for metal film, metal oxide, and carbon film construction resistors. The metal film and carbon film resistors show a $t^{-1/2}$ power dependancy over the test range while the metal oxide resistor shows a t^{-1} dependancy. The significance of these differences cannot be assessed directly from the test data. However, they are important for the theoretical effort.

An important point in evaluating failure modes is the definition of failure. The test data indicates a very gradual change in resistance. Changes on the order of 1% to 10% are clearly defined, and it is possible

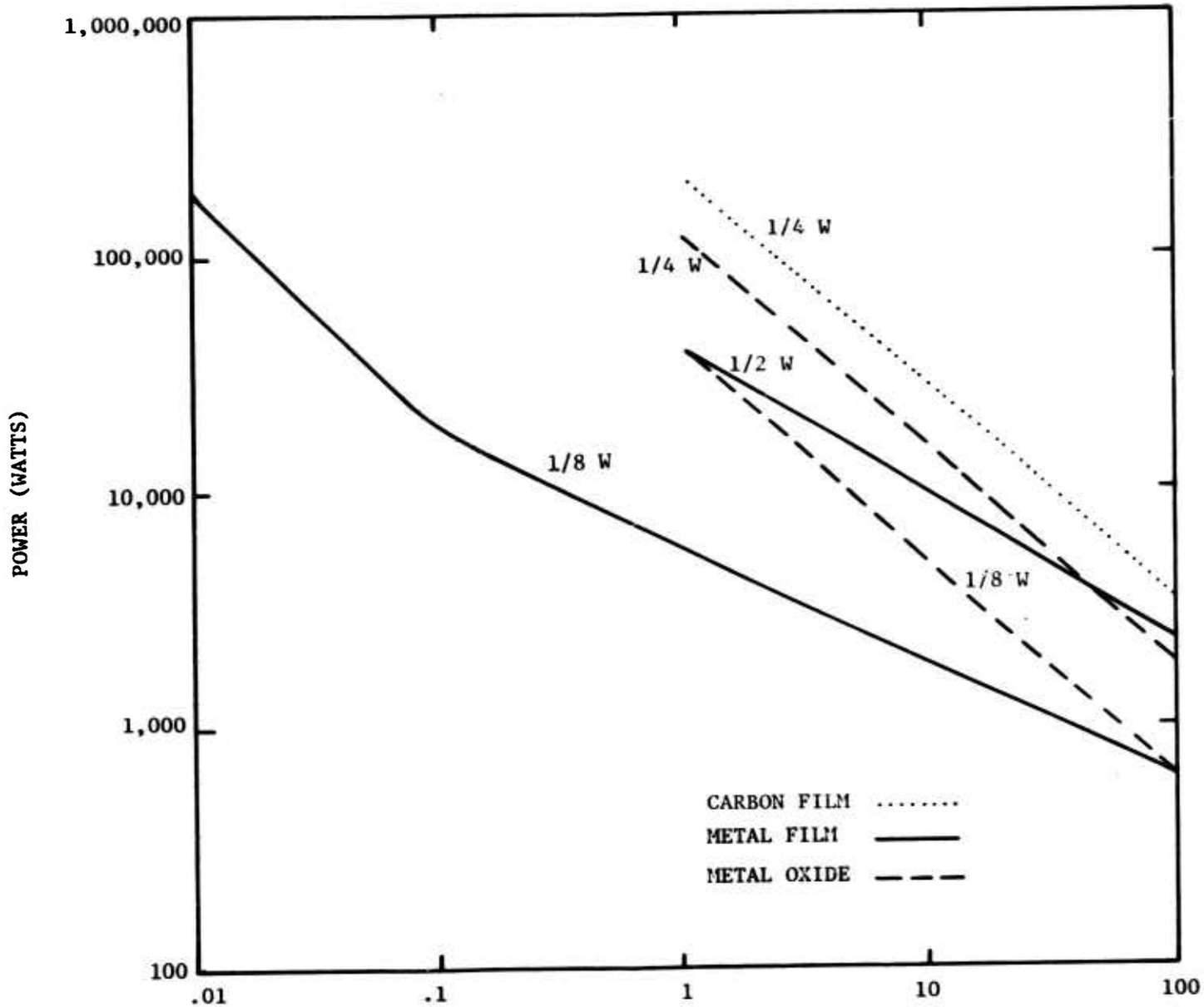

Figure 9. Failure Power Versus Pulse Width for 50 Ω Resistors

to test a substantial resistor sample and maintain a 10% degradation for nearly the entire sample, even though a wide range of failure powers may be observed. For resistance changes greater than 10%, the amount of power required to achieve a given degradation is not consistent. For some resistor types doubling the applied power may only change the resistance a factor of two, while for other types it may result in a change of a factor of ten or more. Since there is no obvious definition of failure, the definition used in this program was based on the specified resistor tolerance. For 1% tolerance resistors a resistance change of 10% was taken as failure. For 10% tolerance a 25% change was taken as failure. This definition is completely arbitrary. The comparison between the power required for a 10% resistance change and power required for a 100% resistance change was seen in Figure 4.

2. FAILURE POWER VERSUS RESISTOR CONSTRUCTION

Five resistor construction types were tested at various pulse widths. Comparison is complicated by the difficulty in obtaining data with all test variables held constant. As indicated in Section II, this difficulty arises due to delays in resistor delivery and to limitations on the pulse generator. However, the following table offers a good general comparison for 1/8 watt, 50 Ω resistors.

			POWER (watts)	
CONSTRUCTION	VENDOR	NUMBER	1 μs	100 μs
Metal Film	Dale	RN55D	6800 W	600 W
Metal Film	TRW	RN55C	-	1600 W
Metal Oxide	Corning	C-4	39500 W	550 W
Carbon Comp	Allen Bradley	RCR05G	-	9400 W
Wire Wound	RCL	7009ER	-	29700*W

* No Fail

The shorter pulse width (1 μs) is the more meaningful for EMP hardness. However, failure data was only attained at 100 μs for the carbon composition and wire wound resistors. Based on this data, the metal film resistor is clearly the softest construction category. This comparison is also seen in Figure 10, which is a plot of the same data and shows the same general trends.

The lowest failure threshold was presented by the RN55D, which is a 1/8 watt metal film resistor. Because of its low failure threshold and also because of the manufacturer's cooperation in supplying data, this resistor was studied extensively in the remainder of the program. The previous table did not consider the carbon film type resistor since no data was obtained for 50 Ω carbon film resistors. The relative hardness can be compared using the following data for 1/8 watt, 13 kΩ resistors with a 10 μs pulse duration.

CONSTRUCTION	VENDOR	NUMBER	POWER
Metal Film	Dale	RN55D	350 W
Metal Oxide	Corning	C-4	3000 W
Carbon Film	Dale	MC1/10	3300 W

The metal film is again seen to be the softest construction category. The carbon film is slighlty harder than the metal oxide. However, it should be noted that the spread in the data was so large that this comparison of averages is not sufficient to distinguish between the metal oxide and carbon film. The distinction can be further illuminated by using data obtained for a slightly different resistor type. This type is the TRW RCR07G. This resistor employs a carbon composition designation number, but it is actually a carbon film type resistor. Comparison of failure data for 1/4 watt, 50 Ω resistors is shown in the following data.

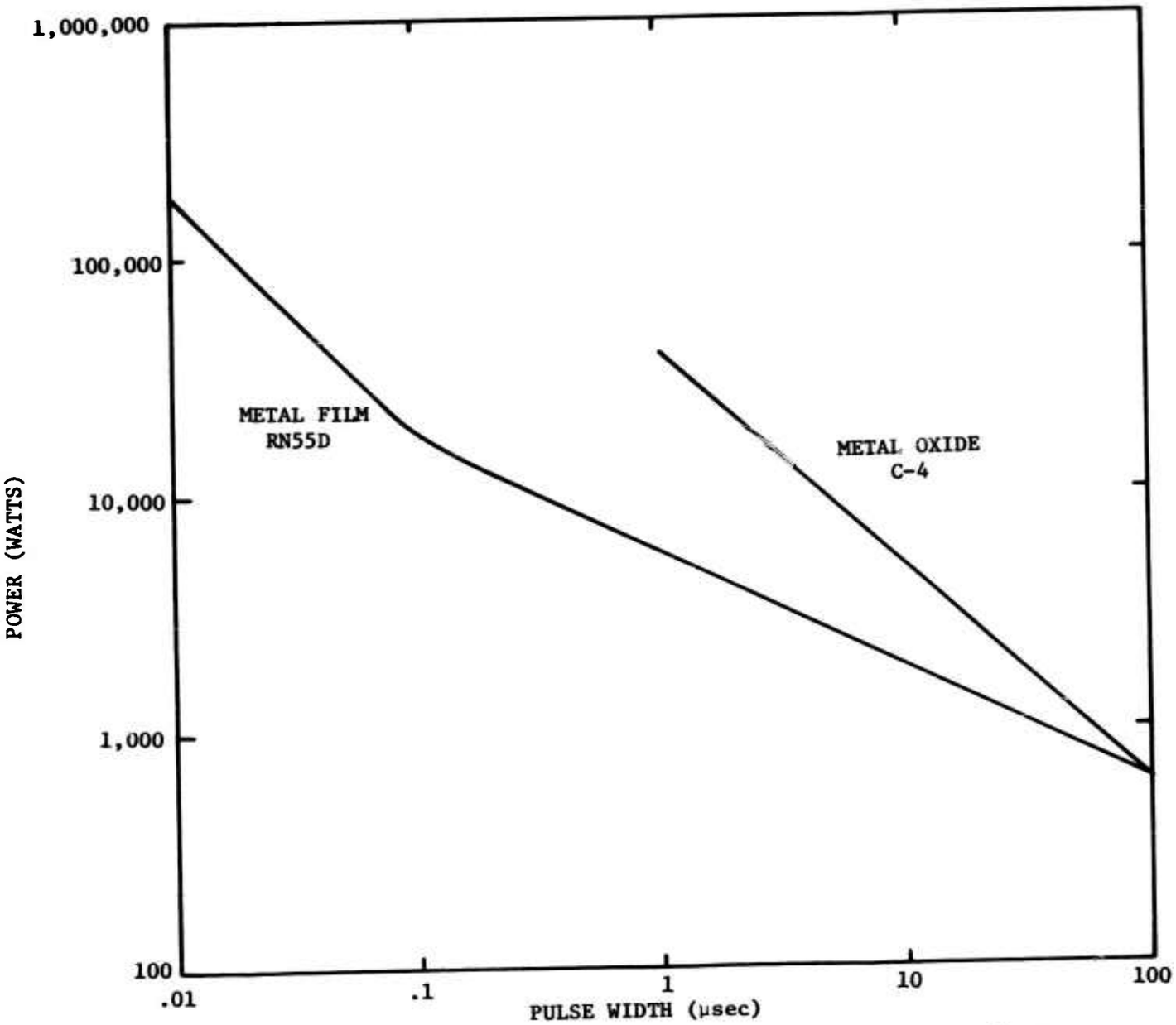

Figure 10. Failure Power Dependence on Construction for 1/8 W, 50 Ω Resistors

CONSTRUCTION	VENDOR	NUMBER	POWER 1 μs	10 μs	100 μs
Metal Film	TRW	RN60C	-	-	1.5 kW
Metal Oxide	Corning	C5	120 kW	15 kW	2 kW
Carbon Film	TRW	RCR07G	220 kW	28 kW	3.7 kW

This comparison confirms the previous observations and also indicates that the carbon film is somewhat harder than the metal oxide construction.

In summary then, the five resistor construction types can be rated in terms of increasing hardness to EMP transients as follows:

(1) Metal Film
(2) Metal Oxide
(3) Carbon Film
(4) Carbon Composition
(5) Wire Wound.

3. FAILURE POWER VERSUS RATED POWER DISSIPATION

As might be anticipated, a strong relation was indicated between failure power and power dissipation rating. Failure test data for 50 Ω, metal film resistors is shown below.

POWER RATED	VENDOR	NUMBER	POWER (watts) 1 μs	10 μs	100 μs
1/8 W	Dale	RN55D	6800	1700	600
1/4 W	TRW	RN60C	-	-	1500
1/2 W	TI	RN65C	41000	10000	2500*
1/2 W	Dale	RN65D	30000	6000	2400
3/4 W	TRW	RN70D	30000	12000	4800*

The asterisk indicates the data is extrapolated from the other pulse widths. Although there are individual inconsistencies, the trend is clear that failure power increases with dissipation power rating for metal film resistors. A similar comparison for metal oxide resistors is shown in Figure 11. This figure shows failure power versus pulse width curves for metal oxide resistors rated at 1/8 and 1/4 watt using three different values of resistance. The 1/4 watt resistor is seen to maintain a consistent factor of three hardness over the 1/8 watt resistor for all pulse widths and resistors values.

4. FAILURE POWER VERSUS RESISTANCE

Two types of relationships were observed between failure power and resistance. One relationship is that exhibited by the metal oxide resistors as shown in Figure 11. The 50 Ω and 200 Ω resistors are seen to be almost identical while the 13 kΩ shows a lower failure power for the only pulse width for which data was obtained. Another relationship is indicated in Figure 12, which plots failure power at 1 μs versus resistance for 1/8 watt and 1/4 watt metal film resistors. The graph connects the average failure power for each resistance value and the spread in the experimental data is indicated by the bars. The trend appears complicated, but the RN55D characteristics, at least, can be explained using the thermal failure model. This curve will be discussed in Section V. In summary, it can be stated that there is no straightforward relationship between resistance and failure power indicated by the data.

5. FAILURE POWER VERSUS MANUFACTURER

A limited study of the correlation of failure power among manufacturers for a given construction technology can be made from the data. The following data presents failure power for 1/2 watt, 50 Ω metal film resistors obtained from three different manufacturers.

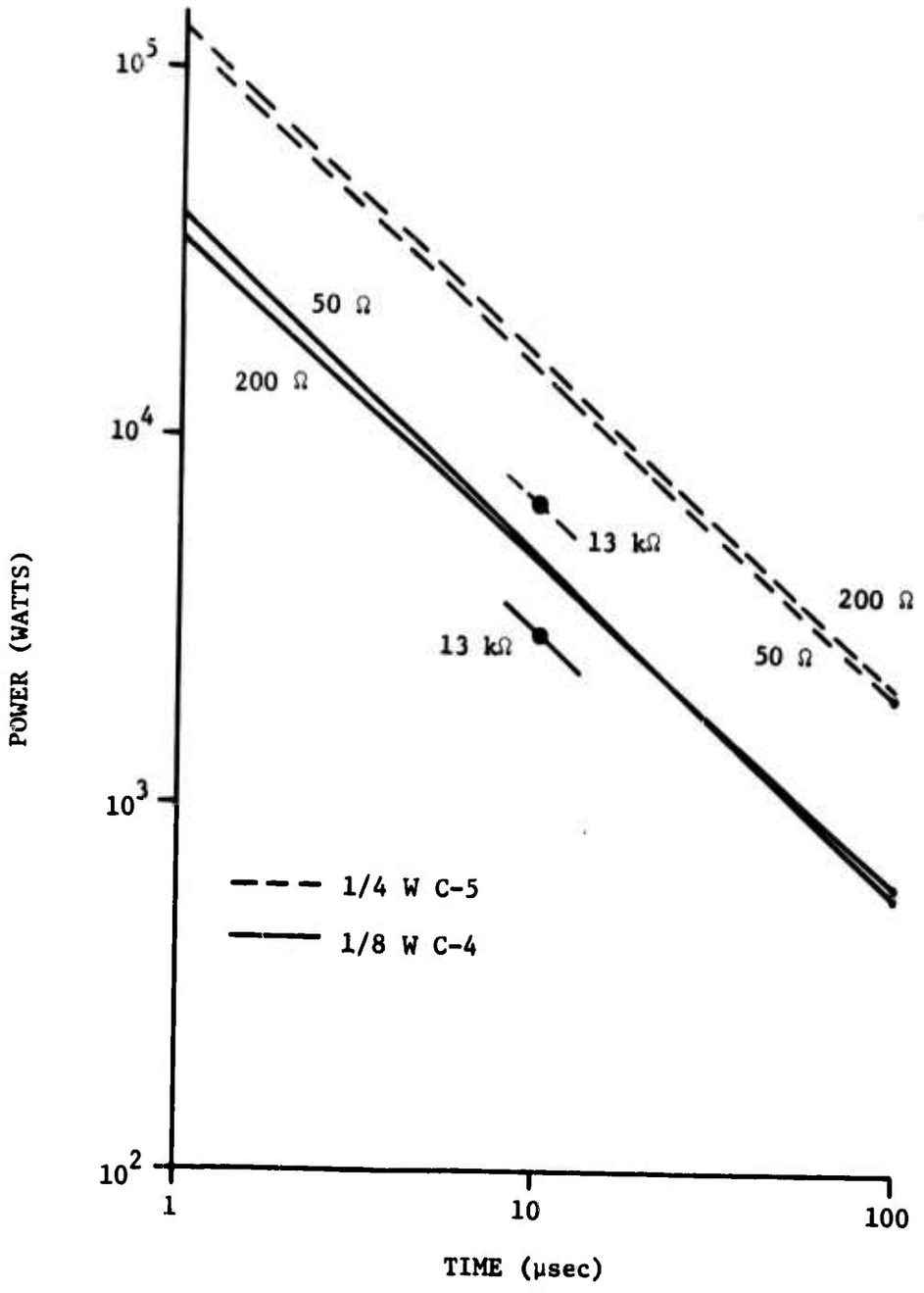

Figure 11. Failure Power Plate for Metal Oxide Resistor

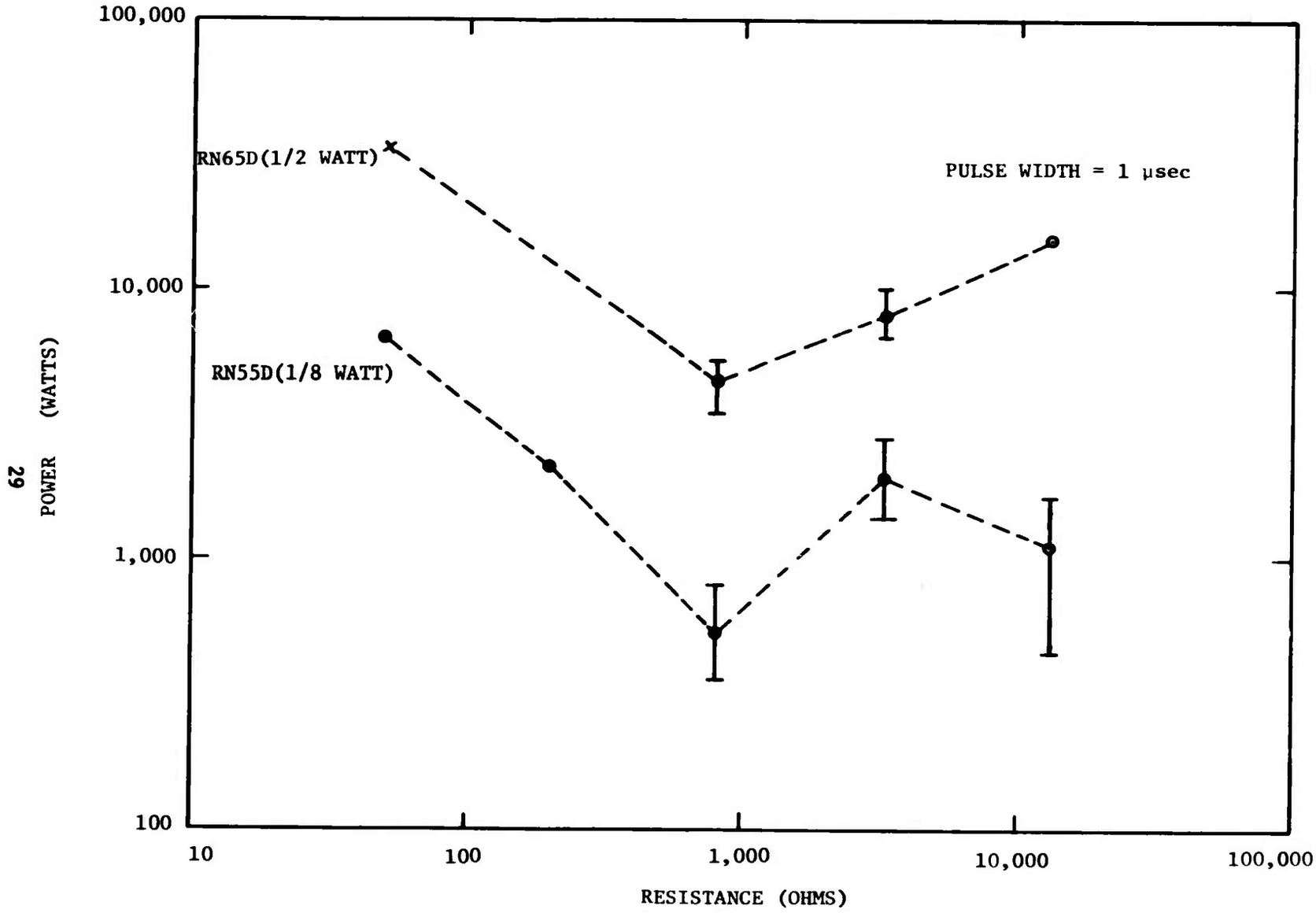

Figure 12. Failure Power Dependence on Resistance for Metal Film Resistors

MANUFACTURER	NUMBER	POWER (watts) 1 μs	10 μs	100 μs
Dale	RN65D	30000	6800	1600
TI	RN65C	40000	10000	2500
TRW	RN65C	-	-	3000

The data is seen to agree well within the measured spread of failure powers. For example, the TRW resistor which showed an average failure power of 3000 watts at 100 μs actually ranged from 1780 watts to 4390 watts. For the same pulse width, the TI (Texas Instruments) resistor ranged from 1650 watts to 3170 watts. The 100 μs power for the Dale resistor is extrapolated from the other two pulse widths.

Thus, it appears that the variations among manufacturers are of the same order as the variations within the test sample itself, and that manufacturer is not an important parameter.

6. ARCING TESTS

A brief series of tests was performed to evaluate the possibility of arcing around a resistor. Tests were performed on metal film, carbon film, and carbon composition resistors. The results are presented in Table 2. The metal film and carbon composition resistors all failed due to power dissipation before arcing was observed. These resistors were observed to withstand in excess of 10 kV without arcing. However, arcing was observed for the carbon film resistor. This resistor (TRW RCR07G) uses a carbon composition number. However, examination of its construction showed that it was actually a carbon film. The carbon film is deposited on a hollow nonconducting cylinder. The electrodes are inserted into the hollow cylinder and are separated by a fraction of an inch. The

Table 2. Arcing Test Summary

CATEGORY	TYPE	RESISTANCE	PULSE WIDTH (μsec)	RESULTS
Metal Film	RN55	30 k	1	No Arc; Power Failure
	RN55	214 k	50	Arc 11-14 kV; Power Failure Progressing Before Arc
	RN70	30k	1	No Arc; Power Failure
Carbon Composition	RC07	27 k	5	1/3 Arced 13 kV; 2/3 no Arc 16 kV
(Slug Construction)	RC07	27 k	15	No Arc 16 kV
	RC07	27 k	40	Body Cracked then Arced 2 kV
	RC42	30 k	1	No Arc 18 kV
	RC42	30 k	10	No Arc 18 kV
Carbon Composition	RC07	3.6 k	10	Arc 2.8 kV → 3.3 kV
(Carbon Film Construction)	RC07	3.6 k	100	Arc 2.8 kV → 3.3 kV

leads thus form a spark gap. Test results indicated that the arc voltage for the spark gap was reasonably consistent at about 3 kV. This type of arcing did not degrade the resistor itself.

Thus, arcing was found to be a function of the electrode configuration rather than the resistor construction or any resistor ratings. All except the carbon film resistor (carbon composition rated) withstood at least 10 kV without arcing. It should be noted that during tests it was discovered that these observations apply only for clean resistors. The presence of any contamination on the resistor can significantly degrade its insulation level.

7. DATA SUMMARY

Table 3 presents a summary of the average failure powers for all resistor types for which failure testing was performed on this program. The average failure power (in kW) is tabulated for three pulse widths (1, 10, and 100 μs). The average power was obtained from a best fit to the power versus time plots. In some cases it was necessary to interpolate or extrapolate on the best fit to obtain the power for the given pulse width. The asterisk indicates that no failure occurred for that entry.

Table 3. Data Summary

	RESISTANCE	CONST.	POWER	TYPE NO.	VENDOR	%	P1	P10	P100
1	12.1 Ω	WW	1/5 W	WWA-24	DALE	0	223 *	-	-
2	49.9 Ω	MF	1/10 W	RN55C	TRW	100	-	-	1.6
3	49.9 Ω	MO	1/8 W	C-4	CORNING	30	39.5	5.7	.55
4	49.9 Ω	MF	1/8 W	RN55D	DALE	10	6.8	1.7	.6
5	49.9 Ω	MF	1/8 W	RN55D	DALE	100	36	9	2.2
6	49.9 Ω	MO	1/4 W	C-5	CORNING	40	120	16	2
7	49.9 Ω	MF	1/4 W	RN60C	TRW	80	-	-	1.4
8	49.9 Ω	MF	1/2 W	RN65C	TRW	100	-	-	3
9	49.9 Ω	MF	1/2 W	RN65C	T1	20	41	10	2.5
10	49.9 Ω	MF	1/2 W	RN65D	DALE	10	30	6.8	1.6
11	49.9 Ω	MF	3/4 W	RN70D	DALE	10	30	12	4.8
12	51 Ω	WW	1/8 W	7009ER	RCL	0	206 *	-	29.7 *
13	51 Ω	CC	1/8 W	RCR05G	A-B	0	294 *	33.9 *	9.5
14	51 Ω	CC/CF	1/4 W	RCR07G	TRW	20	240	30	3.7
15	200 Ω	MO	1/8 W	C-4	CORNING	60	36	4	.6
16	200 Ω	MF	1/8 W	RN55D	DALE	10	2	.7	-
17	200 Ω	MO	1/4 W	C-5	CORNING	30	130	17	2
18	200 Ω	CC/CF	1/4 W	RCR07G	TRW	20	29.0	10	2.5
19	200 Ω	CF	1/2 W	MC1/4	DALE	10	35.	15	5
20	200 Ω	MF	3/4 W	RN70D	DALE	10	15	4	1
21	806 Ω	MF	1/8 W	RN55D	DALE	10	.6	-	-
22	806 Ω	MF	1/2 W	RN65D	DALE	10	4.	-	-
23	3.24 KΩ	MF	1/8 W	RN55D	DALE	10	2.	-	-
24	3.24 KΩ	MF	1/2 W	RN65D	DALE	10	8.	-	-
25	13 KΩ	MO	1/10 W	C-3	CORNING	30	-	.3	-
26	13 KΩ	MO	1/8 W	C-4	CORNING	50	-	3	-
27	13 KΩ	MF	1/8 W	RN55D	DALE	10	1.5	.35	.15
28	13 KΩ	CF	1/8 W	MC1/10	DALE	40	-	3	-
29	13 KΩ	MO	1/4 W	C-5	CORNING	40	-	6	-
30	13 KΩ	MF	1/4 W	RN60C	TRW	25	-	4	-
31	13 KΩ	MF	1/2 W	RN65D	DALE	10	1.5	-	-
32	13 KΩ	CF	1/2 W	MC1/4	DALE	38	-	12	-

*No Fail

SECTION IV

RESISTOR MODELING

1. GENERAL

This section describes the analytical effort to develop a theoretical model for the failure of a metal film resistor. The metal film resistor was chosen since the experimental data had shown it to exhibit the lowest failure threshold. A basic requirement for a theoretical model is to know the physical construction characteristics of the object to be modeled. Considerable effort has expended, without success, in trying to remove the epoxy coating which covers the resistive material in order to observe the construction. It was therefore necessary to gather detailed information on resistor construction and processes, and to postulate resistor failure mechanisms based on this information and known material failure properties. General literature references and manufacturer's catalogs and application notes provided some of the needed information. In addition, personnel at The Boeing Aerospace Company and at DALE Electronics provided more detailed information.

A brief discussion of the construction processing methods as they relate to the theoretical model development follows.

The metal film resistor is composed of three parts:

(1) A cylindrical substrate of Al_2O_3. (This is not the only substrate material that could have been chosen, but it is typical.)
(2) A thin resistive film of nichrome deposited on the substrate.
(3) An epoxy coating on top of the nichrome film.

The nichrome film is placed upon the substrate by vacuum deposition. A cylindrical section of substrate is placed in a vacuum chamber along with a nichrome blank. The blank is heated until a portion is vaporized. The vapor coming in contact with the substrate quickly cools and adheres to the substrate. The thickness of the film so deposited depends on the deposition rate and the length of time the substrate is exposed. This method results in very thin films, on the order of 100-1000 angstroms thick. Because of the complete contact between film and substrate, they are generally assumed to be in intimate thermal contact.

Possible effects of the above manufacturing process on the resistive film include:

(1) The formation of a thin layer of insulating metal oxide between the resistive film and substrate.

(2) A chrome-rich inner layer to the resistive film. This occurs if the blank is not flash heated, then more chrome than nickel will be initially in the vapor.

(3) A variable film thickness because of substrate surface irregularities.

The possible effects of these factors on the resistor failure may impact the accuracy of the treatment to follow.

2. THERMAL MODEL CONSIDERATIONS

The resistive film will be a heat source when a voltage is applied to the resistor while the substrate acts as a heat sink. The epoxy can be ignored since its heat sinking capabilities are far inferior to those of the substrate. The behavior of the heat flow is described by a set of

differential heat flow equations subject to a set of boundary conditions determined by the physical configuration. For this problem, one condition is that the film does not interact with the outside atmosphere and another is that it is in intimate thermal contact with the substrate. The equations are solved by the use of Laplace transforms. Because of the cylindrical geometry of the resistor, the equations are treated in a cylindrical coordinate system.

Resistor failure is assumed whenever the temperature of the electrically resistive material reaches its melting temperature. This definition of resistor failure threshold is based on the assumptions that (1) the melting temperature of the substrate is greater than the melting temperature of the resistive material, (2) melting of any encapsulating material does not significantly degrade the performance of the resistor, and (3) the thermal expansion characteristics of the resistor are not of consequence over the expected dynamic range of temperatures.

The time history of the temperature of a material or a composite of materials at any point within the volume of space occupied by the material is characterized by differential equations of the form

$$K\nabla^2 v + \frac{\partial K}{\partial v} (\nabla v)^2 - \rho c \frac{\partial v}{\partial t} = -Q \qquad (1)$$

In Equation 1, $v(\underset{\sim}{r}, t)$ is the temperature at the point $\underset{\sim}{r}$ and time t, K is the thermal conductivity of the material (assumed independent of $\underset{\sim}{r}$), ρ is the density, c is the specific heat and Q is the heat production per unit time per unit volume in the material.

If the thermal conductivity of the material(s) is not a function of temperature, then Equation 1 reduces to the standard form

$$\nabla^2 v - \frac{1}{k} \frac{\partial v}{\partial t} = -Q/K \tag{2}$$

where $k = K/\rho c \equiv$ diffusivity of the material. In addition, if K is not a function of temperature and Q is at worst a linear function of temperature, then Equation 2 is separable (within geometric constraints) and analytical solutions of Equation 2 are possible. For more complex, composite material configurations, these solutions are generally in the form of integral equations which must be solved by numerical methods.

Since large ranges of temperatures are found, the thermal properties of the material(s) are generally functions of temperature. In addition, the electrical resistance of most resistive material depends upon temperature. As a consequence, the differential equation is nonlinear and the probability of finding analytical solutions becomes negligible unless the linear terms are second-order or average values for thermal properties and source terms can be used.

In some instances, a change of variable

$$\Theta = \frac{1}{K_o} \int_o^v K dv \tag{3}$$

where K_o is the value of K when $v = 0$, may be used to reduce the nonlinear Equation 1 to a simpler form. With this change of variable, Equation 1 becomes

$$\nabla^2 \Theta - \frac{1}{k} \frac{\partial \Theta}{\partial t} = - Q/K_o \tag{4}$$

If c/K is approximately constant and Q does not depend on V, then Equation 4 is linear or amenable to perturbation techniques. However, if none of the above conditions are satisfied, then Equation 1 must be solved directly using numerical techniques because superposition is no longer valid, and in all but a very few cases, the method of separation of variables is not applicable to nonlinear differential equations.

Solutions to Equations 1, 2, and 4 have physical meaning only if prescribed initial and boundary conditions exist. For the purpose of this study, heat transfer due to radiation will be neglected. Therefore, the following boundary conditions are appropriate:

(1) For an air-material interface, it is assumed that there is no heat flux across the surface of the interface, i.e.,

$$\frac{\partial v}{\partial n} = 0, \text{ at all points of the surface,}$$

where $\frac{\partial v}{\partial n}$ denotes differential in the direction of the outward normal to the surface.

(2) For a material-material interface it is assumed that both the temperature and heat flux are continuous across the surface of the interface, i.e.,

$$v_1 = v_2 \text{ and } K_1 \frac{\partial v_1}{\partial n} = K_2 \frac{\partial v_2}{\partial n}$$

at all points of the surface.

If nondestructive melting occurs, such as might be anticipated at the boundary between the resistor and the encapsulant, the boundary conditions are significantly modified. First, the melted region must be treated as a distinct material. Second, the surface of separation between the melted and solid material moves and its motion must be determined. In addition,

the boundary conditions between the liquid and solid phases at the surface of separation become

$$v_1 = v_2 = T_1 \text{ and } K_1|\nabla v_1| - K_2|\nabla v_2| = L\rho \frac{\alpha v_1/\alpha t}{\nabla v_1}$$

where T_1 is the melting point of the substance and L is the latent heat of fusion. It is interesting to note that the second boundary condition is nonlinear, introducing additional mathematical complexities.

3. HOMOGENEOUS MODEL

The simplest model is a homogeneous isotropic block of material with uniform heating. Assume that the heat source, Q, is of the form $Q = Q(v)$ for $t > 0$ and $Q = 0$ for $t < 0$. With these assumptions, Equation 1 reduces to

$$\rho c(v) \frac{dv}{dt} = Q(v) \tag{5}$$

Solutions of this equation are trivial and are of the form

$$t/\rho = \int_{v_o}^{v} \frac{c(v)}{Q(v)}\, dv \tag{6}$$

where v_o is the temperature of the material at $t = 0$.

The film material, based on information supplied by the resistor manufacturer, is considered to be composed mainly of a nickel chrome alloy, Nichrome V (77.4 percent Ni, 19.5 percent Cr, 1.4 percent Si, 0.59 percent Mn, 0.45 percent Fe, 0.04 percent C), along with a small percentage of other materials used for "doping" purposes. A melting point of 600°C was chosen for this film material. Complete thermal specifications for Nichrome V are contained in the Appendix. From these specifications, the functional behavior of the Q(v) and c(v) of the film can be derived.

Q(v) is inversely proportional to resistivity; as for a fixed voltage pulse $P = V^2/R$. From Graph A-1 of the Appendix, it can be seen that for straight nickel chrome alloys of 18 percent Cr content or higher, the resistivity is nearly constant. Nichrome V has only trace materials other than nickel and chromium and a chrome content of approximately 20 percent. Therefore a constant resistivity with temperature is assumed for Nichrome V. The same dependence is assumed to hold for the film material comprising the block.

Q(v) is then a constant and Equation 6 can be written as

$$Q = \frac{\rho}{t} \int_{v_o}^{v} c(v)\,dv \tag{7}$$

All that is needed to solve Equation 7 is the functional form of c(v). From Graph A-2 of the Appendix, it can be seen that c(v) for Nichrome V is linear over a broad range of temperatures (550°R - 2250°R). Thus, c(v) can be assumed to be linear over all temperatures of interest, and can be expressed as

$$c(v) = av+b \tag{8}$$

where

$$a = 2.41 \times 10^{3} \text{ ergs/g(°K)}^{2}$$

$$b = 3.70 \times 10^{6} \text{ ergs/g(°K)}$$

The heat required to melt the resistive block can be computed as a function of time by setting $v = v_m = 600°C$, $v_o = 25°C$, $\rho = 8.2 \frac{\text{gms}}{\text{cm}^3}$, and inserting Equation 8 into Equation 7 to yield

$$Q = \frac{\rho}{t} \left[\frac{1}{2} a(v_m - v_o)^2 + b(v_m - v_o) \right]$$

$$= \frac{2 \times 10^{3} \text{ joules/cm}^3}{t}$$

For a 50 Ω RN55D resistor, the film volume is estimated to be 1.98×10^{-6} cm^3. Thus, the total failure power, P, can be expressed as

$$P = 4 \times 10^{-3} \, t^{-1} \text{ watts} \qquad (9)$$

4. COMPOSITE MODEL

Of course, a real metal film resistor is not a homogeneous block. Rather it has a more complex geometry. The next step in complexity is to model the substrate with the proper cross-sectional geometry. Figure 13 illustrates the cross section of an infinite cylinder. Region I is the substrate (K_1, k_1) and Region II is the metal film (K_2, k_2).

Initial temperature is assumed to be 0°C in both regions. Heat production at a constant rate Q_o per unit time per unit volume is assumed in Region II for $t > 0$.

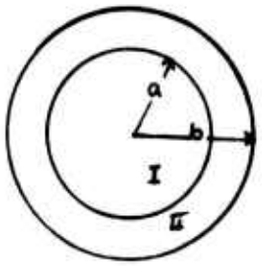

Figure 13. Cross Section of Infinite Composite Cylinder

Writing v_1 and v_2 for the temperatures in the two regions, the subsidiary equations are

$$\frac{d^2 \bar{v}_1}{dr^2} + \frac{1}{r} \frac{d\bar{v}_1}{dr} - q_1^2 \bar{v}_1 = 0 \text{ for } 0 \leq r < a \tag{10a}$$

$$\frac{d^2 \bar{v}_2}{dr^2} + \frac{1}{r} \frac{d\bar{v}_2}{dr} - q_2^2 \bar{v}_2 = \frac{-Q_o}{K_2 P} \text{ for } a < r \leq b \tag{10b}$$

where $\bar{v}_1$ and $\bar{v}_2$ are the Laplace transforms of v_1 and v_2 respectively, p is the Laplace transform independent variable, $q_1 = \sqrt{p/k_1}$ and $q_2 = \sqrt{p/k_2}$. Solving the above equations consistent with the boundary conditions

$$\bar{v}_1(a,p) = \bar{v}_2(a,p)$$

$$K_1 \frac{d\bar{v}_1}{dr}\Big|_{r=a} = K_2 \frac{d\bar{v}_2}{dr}\Big|_{r=a}$$

$$\frac{d\bar{v}_2}{dr}\Big|_{r=b} = 0$$

and requiring $\bar{v}_1$ to be finite at r = 0, yields the following

$$\bar{v}_1 (r,p) = A_1 I_o(q_1 r) \tag{11a}$$

$$\bar{v}_2 (r,p) = \frac{k_2 Q_o}{K_2 p^2} + B_1 [I_o(q_2 r) + \alpha K_o(q_2 r)] \tag{11b}$$

where I_o and K_o are the zeroth-order modified Bessel and Hankel functions respectively and

$$\alpha = I_1(q_2 b)/K_1(q_2 b)$$

$$B_1 = \frac{K_1 q_1 k_2 Q_o}{K_2 p^2} I_1(q_1 a) K_1(q_2 b) / \Big\{ K_2 I_o(q_1 a)$$

$$x[I_1(q_2 a) K_1(q_2 b) - I_1(q_2 b) K_1(q_2 a)]$$

$$-k_1 q_1 I(q_1 a)[I_o(q_2 a) K_1(q_2 b) + I_1(q_2 b) K_o(q_2 a)]\Big\}$$

$$A_1 = \frac{K_2 q_2 B_1}{K_1 q_1} \left[\frac{I_1(q_2 a) - \alpha K_1(q_2 a)}{I_1(q_1 a)} \right]$$

The time history of the temperature may now be obtained by using the Inversion Theorem for the Laplace transformation, i.e.,

$$v(t) = \frac{1}{2\pi i} \int_{\gamma - i\infty}^{\gamma + i\infty} e^{\lambda t} \bar{v}(\lambda) d\lambda \tag{12}$$

where γ is chosen such that all the singularities of $\bar{v}(\lambda)$ lie to the left of the line $(-\infty, +i\infty)$.

Only the temperature of the resistive material is of interest. Therefore, only v_2 need be considered. The highest temperature is expected to occur at r = b or

$$\bar{v}_2\ (b,p) = c_1\left[1+c_2 I_1(q_1a)/\left\{K_2q_2 I_o(q_1a)A-K_1q_1 I_1(q_1a)B\right\}\right] \tag{13}$$

where

$$c_1 = k_2Q_o/K_2p^2$$

$$c_2 = q_1K_1/q_2b$$

$$A = I_1(q_2a)\ K_1(q_2b)\ -I_1(q_2b)K_1(q_2a)$$

$$B = I_o(q_2a)\ K_1(q_2b)+\ I_1(q_2b)K_o(q_2a)$$

This expression for v_2 (b,p) may now be simplified. Assume:
(1) A and B are small and can therefore be expanded in a Taylor Series;
(2) q_1a is so large that $I_o(q_1a)$ and $I_1(q_1a)$ both approach $\frac{e^{q_1a}}{\sqrt{2\pi q_1a}}$
(i.e., only short times are considered)

Expanding A and B about a,

$$A(q_2a,q_2b) = A(q_2a,q_2a)+\dot{A}\ (q_2a,q_2a)\ \Delta q_2+\ \ddot{A}\ (q_2a,q_2a)\ \frac{(\Delta q_2)^2}{2}\ +\ldots$$

$$= 0-\frac{\Delta}{a}\ +\ \frac{\Delta^2}{2a^2}\ -\ \ldots$$

$$\simeq -\ \frac{\Delta}{a}$$

$$B(q_2a,q_2b) = B(q_2a,q_2a)+\dot{B}\ (q_2a,q_2a)\Delta q_2+\ddot{B}\ (q_2a,q_2a)\ \frac{(\Delta q_2)^2}{2} +\ldots$$

$$= \frac{1}{q_2a} - \frac{\Delta}{q_2a^2} +\ldots$$

$$\simeq \frac{1}{q_2a}$$

where $\Delta = b-a$

Using the assumptions, $\bar{v}_2$ becomes

$$\bar{v}_2(b,p) = c_1\left[1-c_2/\left\{ K_2q_2\ \frac{\Delta}{a} + \frac{k_1q_1}{q_2a}\right\}\right]$$

$$= c_1\left[1-c_2\left(\frac{q_2a}{K_2q_2^2\Delta+K_1q_1}\right)\right] \qquad (14)$$

Let $q_2 \equiv q = \left(\frac{p}{k_2}\right)^{1/2}$ then, $q_1 = q\left(\frac{k_2}{k_1}\right)^{1/2}$ so that

$$c_1 = \frac{k_2\ Q_o}{K_2\ p^2} = Q_o/K_2q^2P$$

$$c_2 = \left(\frac{k_2}{k_1}\right)^{1/2}\ \frac{K_1}{b}$$

To a good approximation

$$\frac{a}{b} \approx 1$$

while from the temperature independent thermal properties given in Appendix A

$$\frac{K_2}{K_1}\left(\frac{k_1}{k_2}\right)^{1/2} \approx 1$$

Therefore, with reasonable accuracy

$$\bar{v}_2(b,p) = c_1\left[1 - \frac{a_o}{q + a_o}\right] = c_1\left[\frac{q}{q + a_o}\right] \qquad (15)$$

$$= \frac{Q_o}{K_2}\left[\frac{1}{pq(q+a_o)}\right] \qquad (16)$$

where $a_o \equiv 1/\Delta$

This can now be Laplace transformed, making use of the Laplace transform tables given in Reference 1. $v_2(b,t)$ is found to be

$$v_2(b,t) = \frac{Q_o}{K_2}\left[a_o^{-2}\, e^{a_o^2 k_2 t}\, \text{erfc}\left(a_o\sqrt{k_2 t}\right) - a_o^{-2} + 2/\sqrt{\pi}\; a_o^{-1}\sqrt{k_2 t}\right]$$

The erfc can be expanded by breaking the expression into two regions based on the argument. Set $\alpha = a_o\sqrt{k_2 t}$ and consider $\alpha < 1$ and $\alpha > 1$.
For $\alpha < 1$:

$$\text{erfc } \alpha = 1 - \frac{2}{\sqrt{\pi}} e^{-\alpha^2} \left[\alpha + \frac{2\alpha^3}{3} + \cdots \right]$$

Returning to the expression for Q and setting $v_2(b,t) = v_m$, the failure temperature

$$Q = \frac{K_2 v_m a_o^2}{e^{\alpha^2} \text{ erfc } \alpha - 1 + \frac{2}{\sqrt{\pi}} \alpha}$$

$$= \frac{K_2 v_m a_o^2}{e^{\alpha^2} \left[1 - \frac{2}{\sqrt{\pi}} e^{-\alpha^2} \left(\alpha + \frac{2\alpha^3}{3} \ldots \right) \right] - 1 + \frac{2}{\sqrt{\pi}} \alpha}$$

So,

$$Q = \frac{K_2 v_m a_o^2}{e^{\alpha^2} - \frac{2}{\sqrt{\pi}} \left(\alpha + \frac{2\alpha^3}{3} \ldots \right) - 1 + \frac{2}{\sqrt{\pi}} \alpha}$$

but for $\alpha < 1$; $e^{\alpha^2} \simeq 1 + \alpha^2$

$$Q \simeq \frac{K_2 v_m a_o^2}{(1 + \alpha^2) - \frac{2}{\sqrt{\pi}} \left(\alpha + \frac{2\alpha^3}{3} \ldots \right) - 1 + \frac{2}{\sqrt{\pi}} \alpha}$$

$$\simeq \frac{K_2 v_m a_o^2}{\alpha^2 + \frac{4\alpha^3}{\sqrt{\pi}\,3} \cdots}$$

Neglecting higher order terms

$$Q \simeq \frac{K_2 v_m a_o^2}{\alpha^2} = \frac{K_2 v_m}{k_2}\, t^{-1} \qquad \text{for } \alpha < 1.$$

For the case $\alpha > 1$

$$\text{erfc } \alpha = \frac{e^{-\alpha^2}}{\alpha\sqrt{\pi}} \left[1 - \frac{1}{2\alpha^2} + \cdots \right]$$

and

$$Q = \frac{K_2 v_m a_o^2}{e^{\alpha^2}\ \text{erfc } \alpha - 1 + \frac{2}{\sqrt{\pi}}\ \alpha}$$

$$= \frac{K_2 v_m a_o^2}{e^{\alpha^2}\ \frac{e^{-\alpha^2}}{\alpha\sqrt{\pi}} \left[1 - \frac{1}{2\alpha^2} + \cdots \right] - 1 + \frac{2}{\sqrt{\pi}}\ \alpha}$$

$$Q \simeq \frac{K_2 v_m a_o^2}{\frac{2}{\sqrt{\pi}}\ \alpha - 1}$$

$$Q \simeq \frac{K_2 v_m a_o^2}{\frac{2a_o}{\sqrt{\pi}}\sqrt{k_2 t} - 1}$$

for $\alpha > 10$

$$Q \simeq \frac{K_2 v_m a_o}{\sqrt{k_2}}\, t^{-1/2}$$

The next question is where do the two time regions cross for the RN55D resistor. Using $a_o^{-1} = 1000$ Å, and $k_2 = 4 \times 10^{-2}$ cm^2/sec, α can be evaluated

$$\alpha = a_o \sqrt{k_2 t} = 1$$

$$t = (a_o^2 k_2)^{-1}$$

$$t = 2.5 \times 10^{-9} = 2.5 \text{ nsec.}$$

Thus for all of the test data the assumption $\alpha > 1$ is appropriate.

Finally, compute the power for total resistor value

$$P = Q\ell c a_o^{-1}$$

where ℓ is the resistor length and c is the circumference.

$$P \simeq \frac{K_2 v_m \ell c}{k_2 a_o} t^{-1} \qquad \text{for } t < 1 \text{ ns}$$

$$P \simeq \frac{K_2 v_m \ell c}{\sqrt{k_2}} t^{-1/2} \qquad \text{for } t > 25 \text{ ns}$$

The intermediate time can be obtained by interpolating between these values. The remaining values required to compute P for the RN55D are $\ell c = .2\ cm^2$, $v_m = 873°\ K$, and $K_2 = 1.5 \times 10^6$ erg/sec cm°K. So,

$$P = 130\ t^{-1/2}\ \text{Watts} \qquad \text{for } t > 25 \text{ ns}$$

$$P = 6.5 \times 10^{-3}\ t^{-1}\ \text{Watts} \qquad \text{for } t < 1 \text{ ns}$$

These formulations are for 1000 Å film thickness which is nominal. It is worthwhile to examine a thicker film (10,000 Å) for comparison to the test data. This makes the equations

$$P = 130\ t^{-1/2}\ \text{Watts} \qquad \text{for } t > 2.5\ \mu s$$

$$P = 6.5 \times 10^{-2}\ t^{-1}\ \text{Watts} \qquad \text{for } t < 100 \text{ ns}$$

SECTION V

DISCUSSION OF RESULTS

The equations derived for the homogeneous and composite models are plotted in Figure 14 along with the experimental data for the RN55D. Experimental data is included for both 10% and 100% change in resistance. The homogeneous model is plotted for film thicknesses of 1,000 angstroms and 10,000 angstroms. The homogeneous model is seen to compare to the shape of the observed power versus time relationship only for the shorter pulse widths. This is to be expected since it is in this time region that the assumption of an isotropic block of material is reasonable. For very short pulse widths the heat generated in the material does not have sufficient time to diffuse away from its source, thus giving rise to uniform heating.

The composite model provides a much better approximation of the observed power versus time characteristics. Specifically, the composite model for 10,000 angstrom film thickness agrees to about a factor of three with the observed data for a 100% change in resistance. The power predicted by the analytical model gives $\approx$100% melting which would probably cause the resistor to fail catastrophically. Clearly, the agreement would be closer if the resistors had been tested for a greater change in resistance. Some of the difference between the theoretical and experimental results can presumably be attributed to the estimates made for the thermal constants. Another source of difference is the estimate of the total resistor volume. Finally, note that the analytical model assumes uniform temperature change. In reality, only the hottest hot-spot in the film is likely to reach melting temperature so it is natural to expect experimental data to show failure at lower temperature.

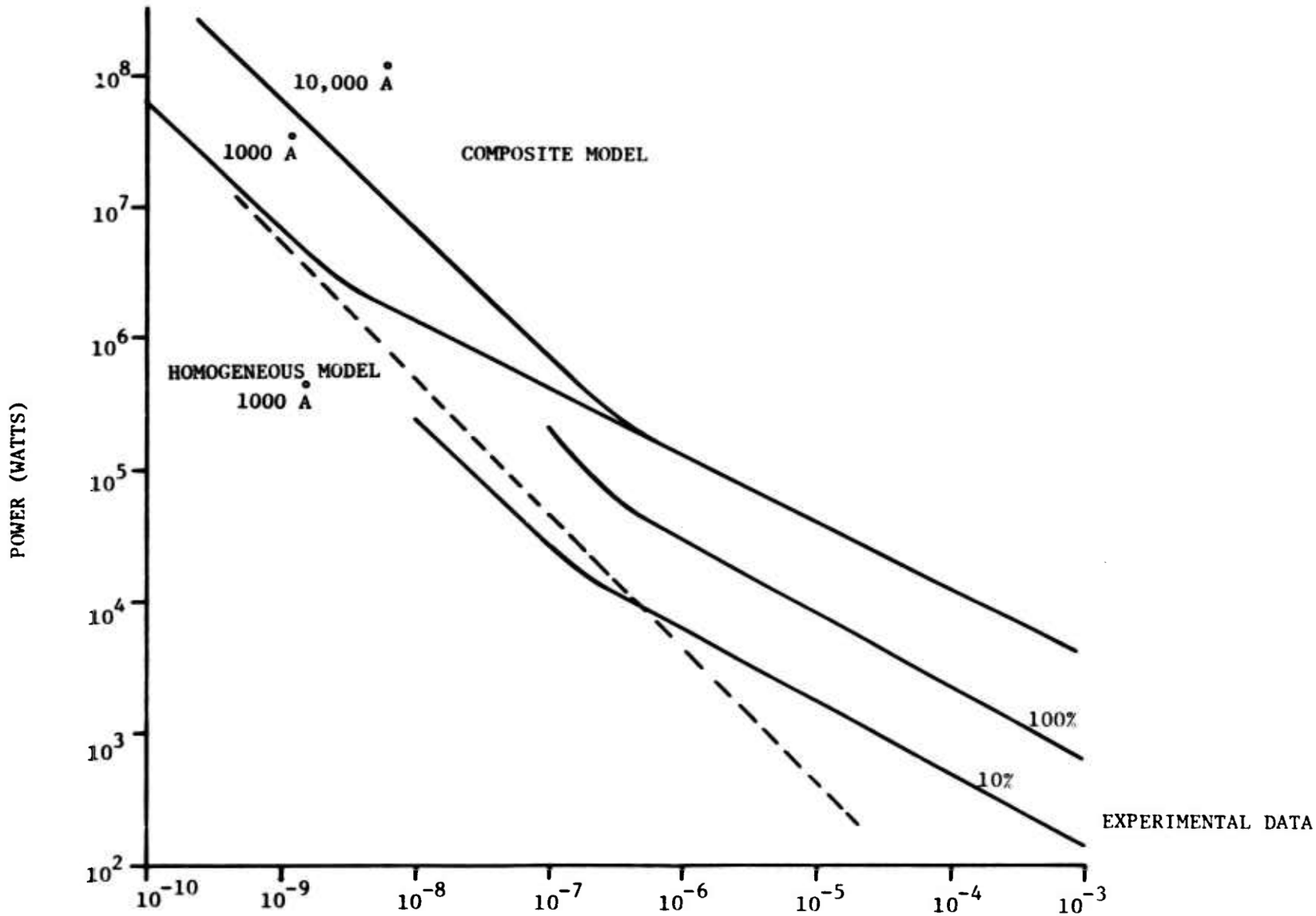

Figure 14. Model Comparison

With these limitations in mind, it can be stated that the composite model is an adequate representation of the experimental data. Thus, the thermal failure mode is appropriate and the correct geometry has been chosen. The composite model could be force fit to the experimental data by adapting an appropriate correction term if desired.

With the available model, and knowledge of the resistor construction, the relationship between power and resistance mentioned in Section III.4 can now be explained. The RN55D consists of a thin film of Nichrome deposited on a cylindrical ceramic slug. A resistive slug is fabricated for a given value (say 50 Ω), and the resistance is increased by scribing-off the Nichrome in a spiral fashion until the desired resistance is achieved. This process is practical only over a range of resistances and thus, in order to increase the resistance beyond that range, a new resistive slug must be fabricated. This higher resistance slug is achieved by reducing the film thickness and, in some cases, changing other parameters. Again, the resistance is increased by scribing-off the Nichrome as before. Discussions with the resistor manufacturer indicate that resistive slugs are changed at 50 Ω and 1 kΩ . Referring back to Figure 12 it is seen that a failure power decreases over the range of 50 Ω to 806 Ω and that the failure power for the 3 kΩ and 13 kΩ resistances is somewhat higher. The inverse relationship between power and resistance for the lower resistances is reasonable since the resistance is being increased by removing some film which in turn reduces the cross-sectional area of the resistor.

Now consider the theoretical failure model. The data being considered here is a 1 μs pulse width for which the long pulse width model is appropriate. So,

$$P = K_2 \, v_m \, \ell c \, k_2^{-1/2} \quad t^{-1/2}$$

Note that there is no dependence of failure power on film thickness. Thus, when the 1 kΩ resistor slug is fabricated by changing the thickness, it has essentially the same failure power as the 50 Ω slug. Again, the film is scribed-off and the failure power decreases with resistance. Of course, changing thickness also changes the thermal time constant somewhat, but this can be ignored for this analysis.

The above discussion implies that the power-resistance product (PR) should be constant for a given resistive slug and that it should vary inversely with the ratio of resistance when slug configuration changes. Thus, assuming the change occurs at 1000 Ω for the RN55D, the PR should be constant up to 1000 Ω, should increase by 1000/50 = 20 at 1000 Ω, and then should remain constant again until the slug configuration changes. This hypothesis can be tested by comparing the values from Figure 12 as follows:

RESISTANCE	POWER	PR	PR/20	V	$V/\sqrt{20}$
50 Ω	6500	325 k	-	650	-
200 Ω	2200	440 k	-	700	-
806 Ω	500	403 k	-	700	-
3.32 kΩ	2000	-	323 k	-	462
13 kΩ	1100	-	660 k	-	760

The agreement is very good. Continuing this analysis it follows that the failure voltage should be constant up to 806 Ω, should decrease by $\sqrt{20}$ at 1 kΩ, and then remain constant again. These values are also provided above. Again, the hypothesis appears to be verified. However, it should be noted that this hypothesis implies a substantial reduction in the volume of the resistive film as resistance increases. It has not been determined whether this does in fact occur for the RN55D.

A final question is the applicability of the composite thermal model to the metal oxide and carbon film resistor types. This question has not been addressed in detail. However, it seems reasonable to assume that the basic geometries of the three resistor types are similar. From this it follows that since metal oxide and carbon film both have a higher resistivity than metal film, they would require a thicker film for a given resistance value. Thus, if the composite model is evaluated for a film thickness of 10 microns (100,000 Å) and the thermal properties and surface area are assumed identical to the metal film resistor, the model approximates the observed data for metal oxide and carbon film resistors. This is shown in Figure 15 which compares experimental data for 1/4 watt, 50 Ω resistors to the model predictions. Since the actual geometry of these resistors is not known, this comparison may not be meaningful. However, it does suggest that with proper attention to physical details, the composite model could be applied to the metal oxide and carbon film resistor types.

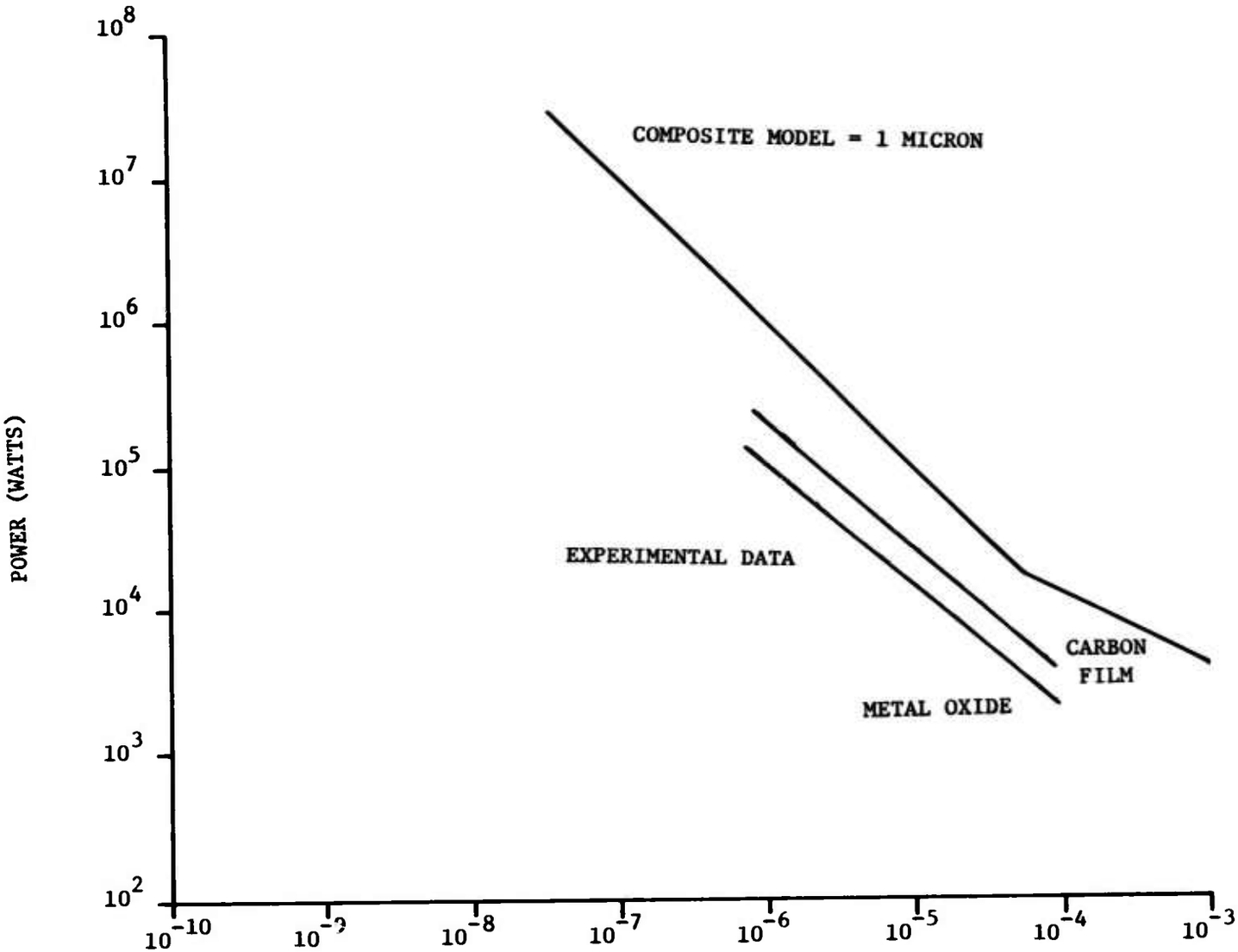

Figure 15. Model Comparison

APPENDIX A

MATERIAL SPECIFICATIONS

Temperature Independent Thermal Properties

Nichrome V

$c_2 = .123$ Btu/lb°R = 5.15×10^6 ergs/g°K

$K_2 = 8.7$ Btu/hr ft°R = 1.50×10^6 ergs/sec cm°K

$\rho_2 = 8.2$ gm/cm^3

$k_2 = 3.56 \times 10^{-2}$ cm^2/sec

Al_2O_3

$c_1 = .250$ Btu/lb°R 10.5×10^6 ergs/g°K

$K_1 = 9.5$ Btu/hr ft°R = 1.64×10^6 ergs/sec cm°K

$\rho_1 = 3.965$ gm/cm^3

$k_1 = 3.94 \times 10^{-2}$ cm^2/sec

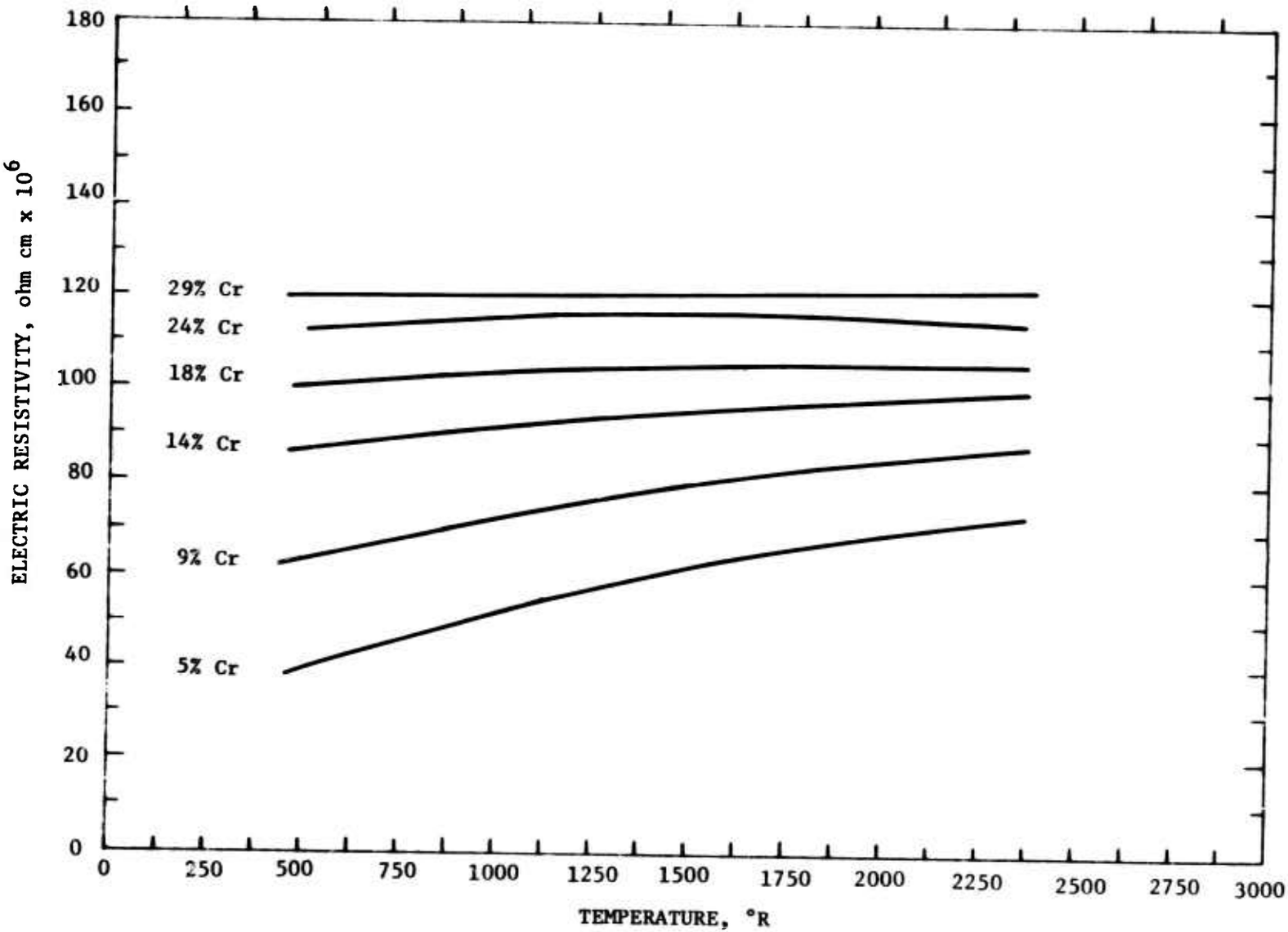

Figure A-1. Electric Resistivity -- Nickel + Chromium

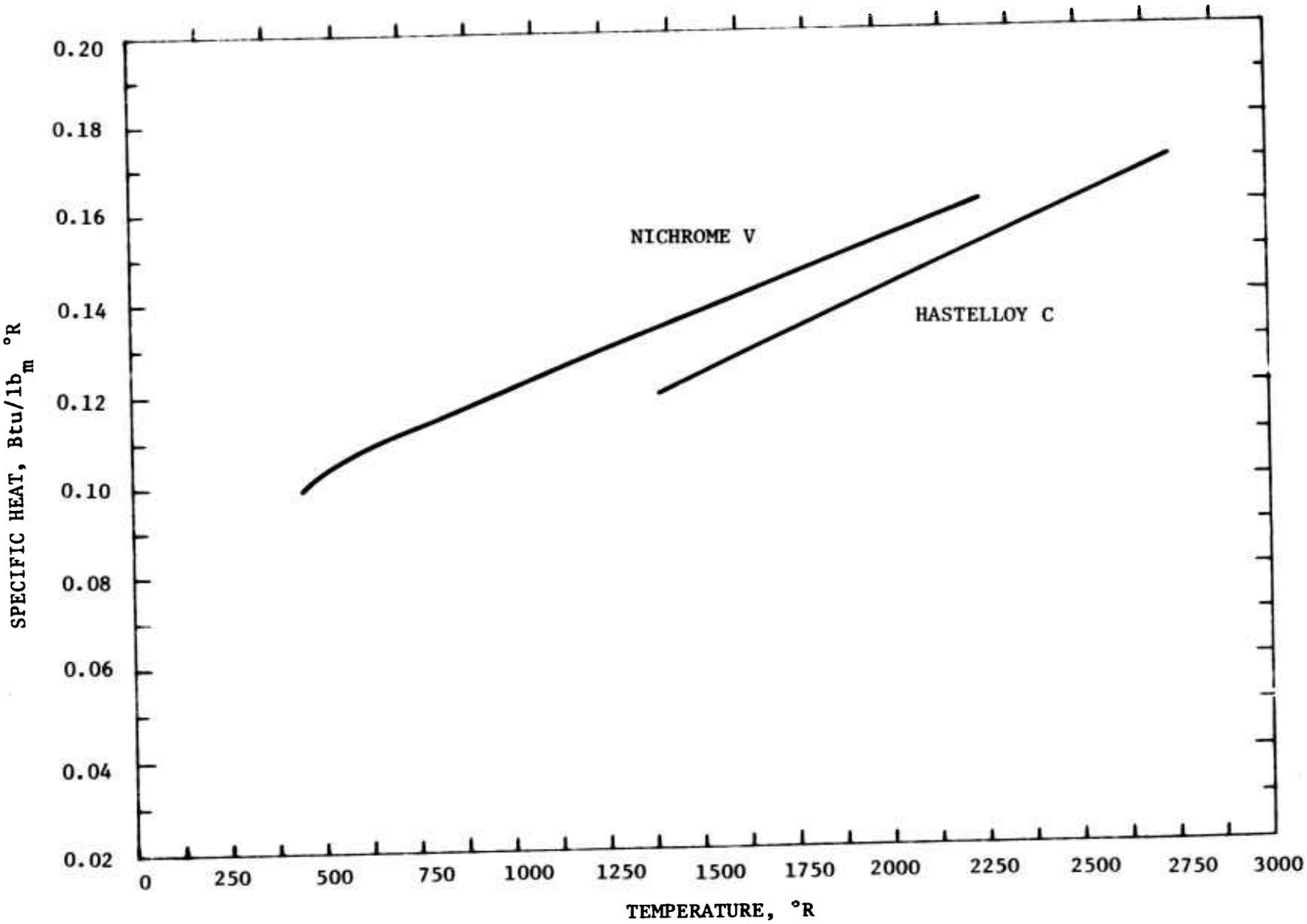

Figure A-2. Specific Heat -- Nickel + Chromium + X

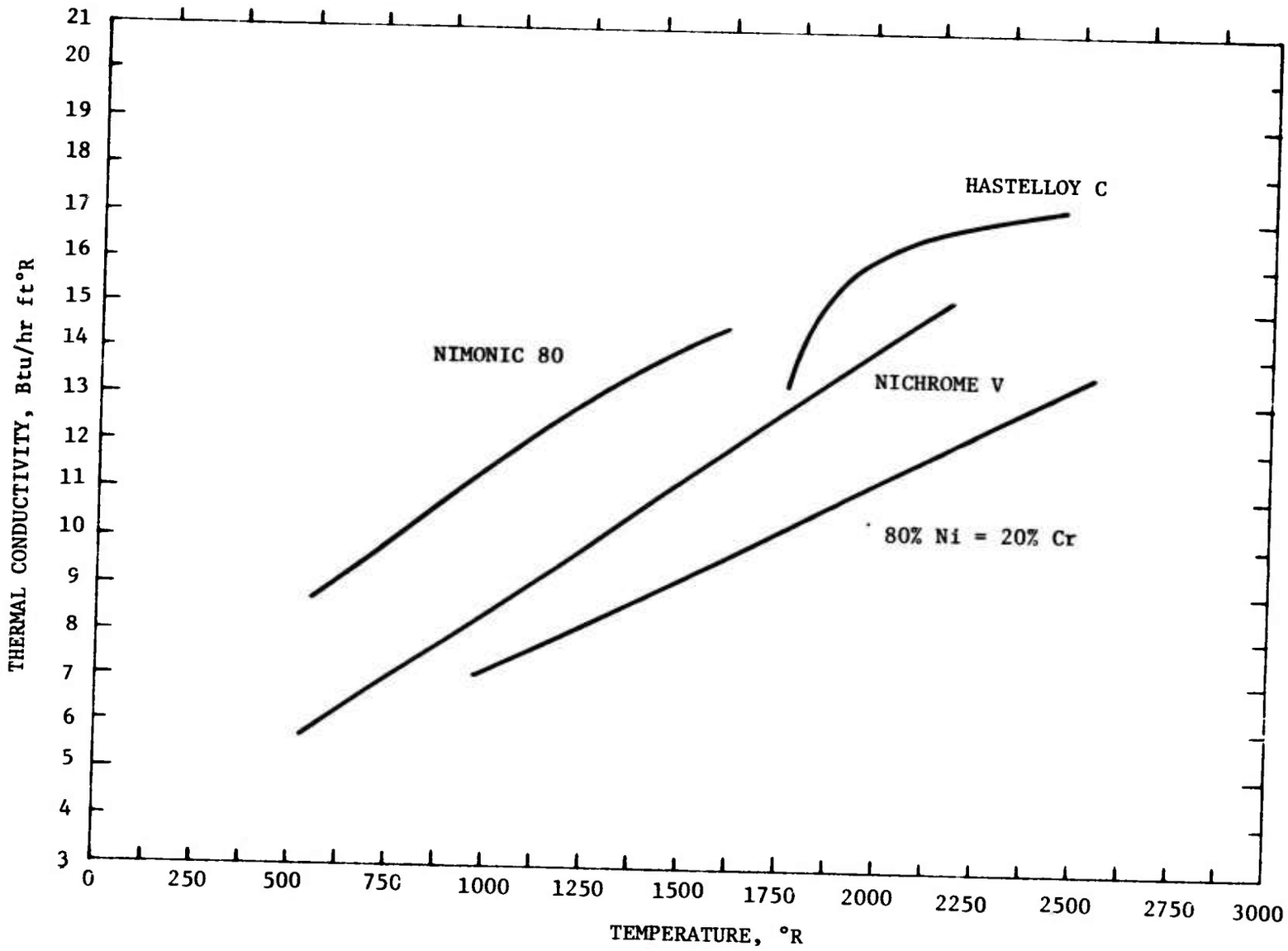

Figure A-3. Thermal Conductivity -- Nickel + Chromium + X

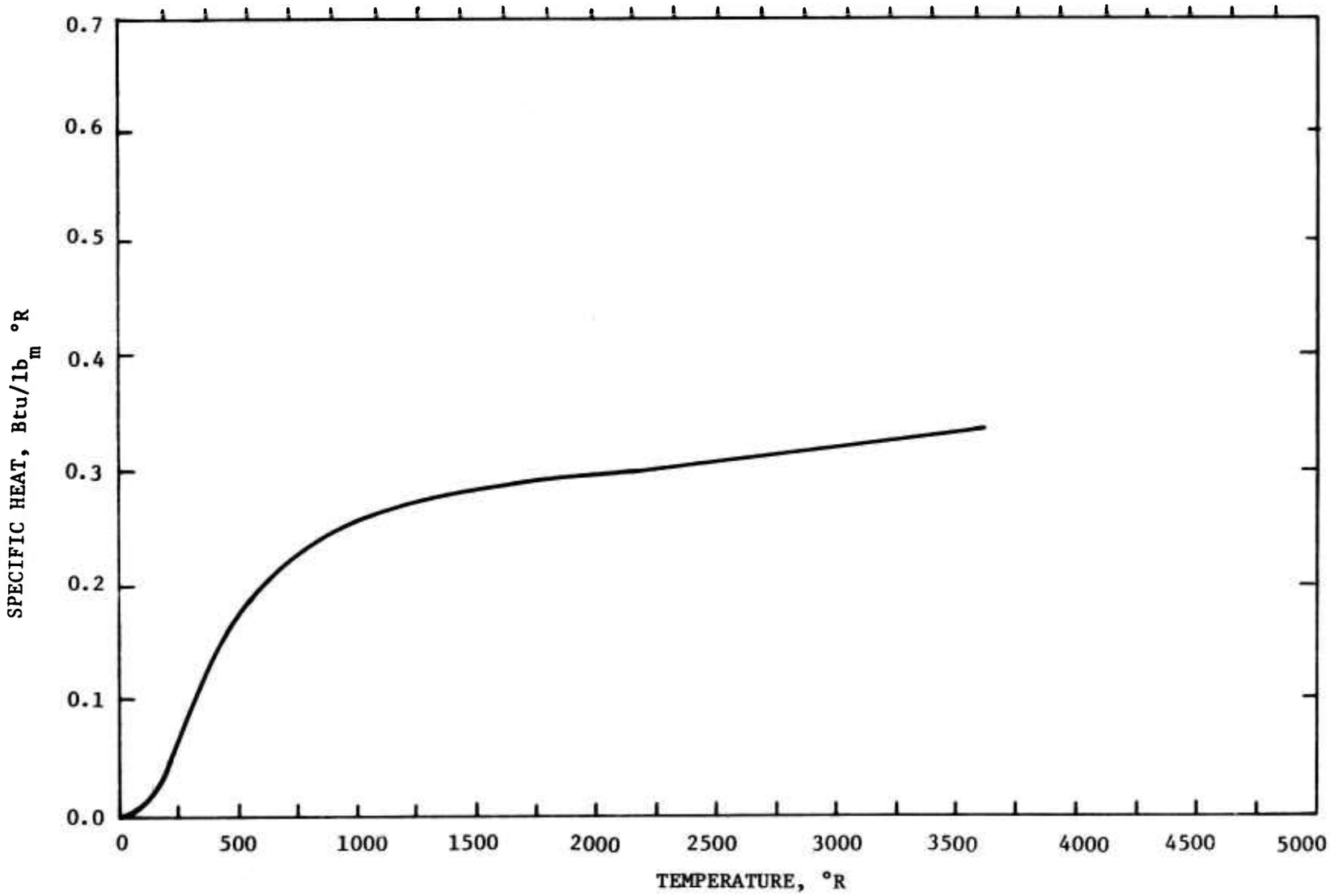

Figure A-4. Specific Heat -- Aluminum Oxide

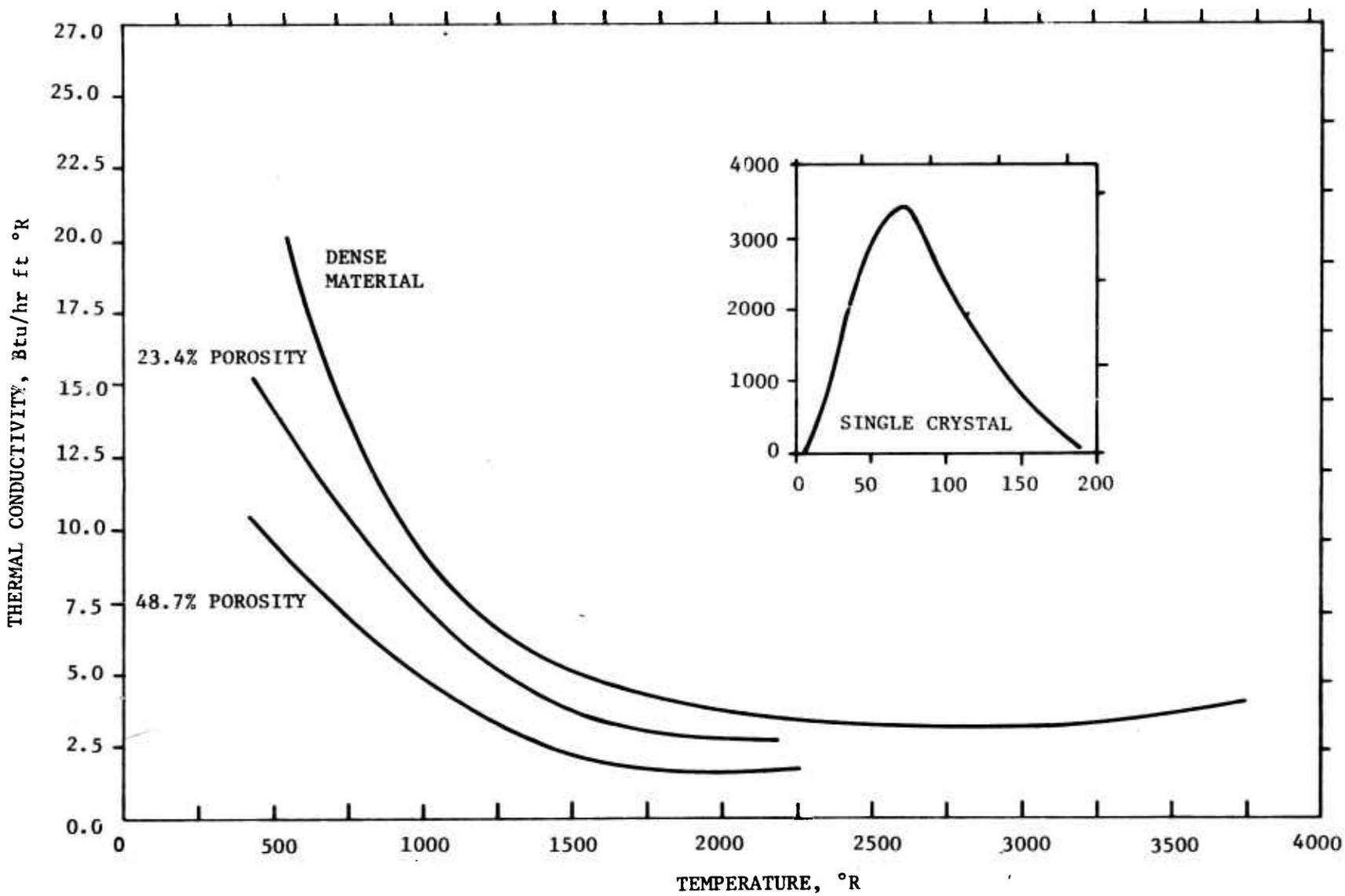

Figure A-5. Thermal Conductivity -- Aluminum Oxide

REFERENCES

1. Conduction of Heat in Solids, H. S. Carslaw and J. C. Jaeger, Oxford University Press, London, 1959.

2. Handbook of Thermophysical Properties of Solid Materials, A. Goldsmith, Wright-Patterson Air Force Base, 1961

DISTRIBUTION LIST

Cdr
Picatinny Arsenal
ATTN: Tech. Lib.

Cdr
NESC
ATTN: Tech. Lib.

Maxwell Lab.
ATTN: Tech. Lib.

DCEC
ATTN: R-124C

DDC
2 cy ATTN: TC

Cdr
DESC
ATTN: ECS/Tech. Lib.

DDR&E
ATTN: Dep. Dir., Strat./Sp. Sys.
ATTN: DAD SK, G. Barse
ATTN: DD/S&SS

Cdr
FC DNA
ATTN: FCPS
ATTN: FCPR

JSTPS
ATTN: Tech. Lib.

Dir.
NSA
ATTN: Tech. Lib.

Dir.
BMDATC
ATTN: Tech. Lib.
ATTN: SSC-TEN, N. Hurst

Ch.
R&D, Dept. of the Army
ATTN: DARD-DDM-N, LTC Goncz

Cdr.
USAMC, RSIC
ATTN: Ch., Doc. Sec.

Cdr
SCA
ATTN: ACCX-SAT-EMP

Cdr
SSSAC
ATTN: Ch., Act. Div.

Cdr.
USA-A
ATTN: NBC Div., AFZT-PTS-C, MAJ Dean

Cdr
USAEC
ATTN: AMSEL-TL-IR, Dr. Hunter

Cdr
ASD
ATTN: Tech. Lib.

Sim. Phys.
ATTN: J. Uglum

CICCADC
ATTN: DCS/C&E, CESA

Cdr
DCA, Nat. Mil. Cmd. Sys. Spt. Ctr.
ATTN: Tech. Lib.

Dir.
DIA
ATTN: Tech. Lib.

Dir.
DNA
ATTN: STSI
ATTN: STVL
ATTN: DDST, P. Haas
3 cy ATTN: STTL
4 cy ATTN: RAEV

Intsvc. Nuc. Wpn. Sch.
ATTN: Doc. Con.

Ch.
FC, DNA, LLL
ATTN: L-395

Ofc. JCS
ATTN: Tech. Lib.

Asst. CS
Com/Elc
ATTN: CEED-7, W. Heath

CE
Dept. of the Army
ATTN: DAEN-MCE-D, Mr. McCauley

Dept. of the Army
FESA
ATTN: Ch., R&T Div.

Cdr
Diamond Lab.
ATTN: AMXDO-EM, A. Renner
ATTN: AMXDO-EM, J. Klebers
ATTN: AMXDO-EM, R. Bostak
ATTN: AMXDO-EM, R. Wong
ATTN: AMXDO-EM, R. Gray
ATTN: AMXDO-RB, J. Miletta
ATTN: AMXDO-RB, E. Conrad
ATTN: AMXDO-NP, S. Marcus
ATTN: AMXDO-NP, F. Wimenitz
ATTN: AMXDO-RBF, J. Tompkins
ATTN: AMXDO-RC, Dr. Oswald
ATTN: AMXDO-RC, TI

Cdr
TRASANA
ATTN: SSEA-EAB, F. Winans

Cdr
USACSC
ATTN: Tech. Lib.

Ch.
USACSA
ATTN: S. Krevsky, DD Eng.
ATTN: Tech. Lib.

Cdr
USAMER&DC
ATTN: Tech. Lib.

Cdr
USANA
ATTN: Tech. Lib.

Ch.
USAN&CSGp
ATTN: MOSG-NO, MAJ Winslow
ATTN: Tech. Lib.

Cdr
WSMR
ATTN: STEWS-TE-NT, M. Squires

OIC
CEL, NCBC
ATTN: Tech. Lib.

CO
NAD
ATTN: Tech. Lib.

Cdr.
NELC
ATTN: Tech. Lib.

Supt.
NPS
ATTN: 2124

Cdr.
NSWC
ATTN: 431, Dr. Malloy
ATTN: E. Dean
ATTN: M. Petree
ATTN: 130-215, E. Rathburn
ATTN: Tech. Lib./Info. Svc. Div.

Cdr.
NWC
ATTN: 753

CO
NWEF
ATTN: ADS

Cdr.
ASD
ATTN: YHEX, Maj Leverette

AFAL
ATTN: DLOSL

AFAL
ATTN: Tech. Lib.

Cdr.
FTD
ATTN: PQAL

SAMSO
ATTN: MN

CICSAC
ATTN: NRI/STINFO
ATTN: XPFS, Maj Stephan

USAEC, NVL
ATTN: CPT Parker
ATTN: Tech. Lib.

Cdr.
USAMC
ATTN: AMSMI-RGP, H. Green
ATTN: AMSMI-RGP, V. Ruwe
ATTN: AMCPM-MD, SAM-D, Proj. Mgr.
ATTN: AMCPM-HA, HAWK, Proj. Mgr.
ATTN: Tech. Lib.

DISTRIBUTION LIST (Continued)

Proj. Mgr.
USATDS
ATTN: Tech. Lib.

Cdr.
USAT&EC
ATTN: Tech. Lib.

Ch.
NOps
ATTN: Tech. Lib.

Cdr.
NASC
ATTN: Tech. Lib.

Cdr.
NCC
ATTN: Tech. Lib.

Cdr.
NOSC
ATTN: ORD-034C, S. Barnham

Dir.
NRL
ATTN: 4004, Dr. Brancato
ATTN: 6603F, R. Statler
ATTN: 2627, D. Folen
ATTN: 6633, J. Ritter
ATTN: Tech. Lib.
ATTN: 7706, J. Boris
ATTN: 7701, J. Brown
ATTN: 464, R. Joiner
ATTN: 7770, D. Levine

Cdr.
NSWC
2 cy ATTN: W. H. Holt
ATTN: FUR, Dr. Amadori
ATTN: Tech. Lib.

Dir.
SSPO
ATTN: Tech. Lib.

ARL
ATTN: Tech. Lib.

Cdt.
AFFDL
ATTN: R. Beavin

CS
USAF
ATTN: RDQPN

Cdr.
RADC
ATTN: Tech. Lib.

LASL
ATTN: Rpt. Lib.
ATTN: K. Riepe, L-1

Sandia Lab.
ATTN: K. Mitchell, 8157

ESD
ATTN: DCD/SATIN IV
ATTN: DCKE, L. Staples
ATTN: YWES
ATTN: XRE-Surv.
ATTN: MCAE, Lt Col Sparks
ATTN: XRP, Maj Gingrich

Sandia Lab.
ATTN: 3141
ATTN: E. Hariman
ATTN: A. Limieux
ATTN: 5223, C. Vittitoe
ATTN: 2126, J. Cooper
ATTN: 1935, J. Gover
ATTN: 9353, R. Parker

CIA
ATTN: RD/SI, Rm. 5G48, Hq. Bldg.
ATTN: Tech. Lib.

NASA
ATTN: ASTR-MTD, A. Coleman, Bldg. 4476

Aerojet El-Sys.
ATTN: T. Hanscome, 8170/D6711

Avco
ATTN: Rsch. Lib., A-830/7201

BMI
ATTN: Tech. Lib.

BPC
ATTN: Proj. Mgr., Gov. Proj., H. Dietze

Bendix Aerosp. Sys. Div.
ATTN: R. Pizarek

Bendix Nav/Cont Div.
ATTN: E. Lademann

BA/H
ATTN: R. Chrisner

CSD Lab.
ATTN: Tech. Lib.

DISTRIBUTION LIST (Continued)

BDM
ATTN: D. Durgin
ATTN: D. Alexander
ATTN: Tech. Lib.

CEC
ATTN: Tech. Lib.

SAMSO
ATTN: SKT, P. Stadler
ATTN: RSP, Lt Col Gilbert
ATTN: DYS, Maj Heilman
ATTN: SZH, Maj Schneider
ATTN: SKD
ATTN: IND, I. Judy
ATTN: DYJB, Capt Ingram
ATTN: SZJ, Capt Dejonckheere

UCC
Holifield Nat. Lab.
ATTN: Dr. D. Nelson
ATTN: Tech. Lib.

UC
LLL
ATTN: Tech. Lib.

Dept. of Commerce
NBS
ATTN: J. French, Elc. Tech. Div.

NASA
ATTN: Library

Aerosp. Corp.
ATTN: Library
ATTN: S. Bower
ATTN: Dr. Pearlston, A2/220
ATTN: R. Murtensen, Hard. Reent. Sys.
ATTN: J. Benveniste
ATTN: Dr. Comisar
ATTN: Dr. Reinheimer
ATTN: I. Garfunkel, 115/2076
ATTN: R. Crolius, A2/1027
ATTN: N. Stockwell, N&E Stf.
ATTN: L. Aukerman, 120/2841
ATTN: V. Josephson, D&S Dir.
ATTN: D. McPherson, Tech. Surv. Dir.

Bell Aerosp.
ATTN: Tech. Lib.

Bell Tel. Lab.
ATTN: Tech. Lib.

Bendix RLD
ATTN: D. Niehaus, Mgr., Pgm. Dev.

Boeing Co.
ATTN: R. Caldwell
ATTN: D. Egelkrout
ATTN: Library
ATTN: Dr. Dye, 2-6005, 45-21
ATTN: H. Wicklein, 17-11
ATTN: A. Lowrey, 2R-00
ATTN: D. Kemle

Brn. Eng.
ATTN: Tech. Lib.

Burroughs Fed/Spec Sys
ATTN: Tech. Lib.

CRC
ATTN: M. Lahr, Library, 106-216

CSC
ATTN: P. Carleston

EG&G
ATTN: Tech. Lib.

FC&IC
ATTN: D. Myers, 2-233
ATTN: Tech. Lib.

Franklin Inst.
ATTN: R. Thompson
ATTN: Tech. Lib.

Gen. Dyn. Corp.
Elc. Div.
ATTN: Tech. Lib.

GE Co., Sp. Div., VFSC
ATTN: L. Chasen
ATTN: J. Peden, CCF 8301
ATTN: D. Tasca, 8301-C8
ATTN: J. Spratt, M9549
ATTN: J. Andrews, Rad. Eff. Lab.
ATTN: TIC

GE Co.
ATTN: B. Showalter, 160

GE Co.
ATTN: Tech. Lib.

GRC
ATTN: Dr. Johnson

Goodyear Aerosp. Corp.
ATTN: B. Manning

GTE Sylv.
ESGp
ATTN: Tech. Lib.

Harris Semicond.
ATTN: Tech. Lib.

Hercules Bacchus Plt.
ATTN: R. Woodruff, 100K-26-W
ATTN: Tech. Lib.

Honeywell Aerosp.
ATTN: H. Noble, Stf. Eng., 725-5A
ATTN: Tech. Lib.

Hughes Acft.
ASD
ATTN: A-1080, W. Scott
ATTN: C-624, E. Smith
ATTN: A-1080, H. Boyte
ATTN: Tech. Lib.

Dikewood
ATTN: Tech. Lib.

Elc. Com.
ATTN: J. Daniel, 9

Fairchild Ind.
SFTC
ATTN: Mgr., CD&S
ATTN: Tech. Lib.

Garrett Corp.
ATTN: R. Weir, 93-9
ATTN: Tech. Lib.

GE Co.
Ord. Sys.
ATTN: D. Corman, 2171

GE Co.
RESD
ATTN: Tech. Lib.

GE Co.
AES
ATTN: Tech. Lib.

GE Co.
TEMPO-Cen.
ATTN: Dr. Rutherford
ATTN: DASIAC

GE Co.
AEG-TIC
ATTN: J. Ellerhorst, E-2

GRC
ATTN: Dr. Hill
ATTN: J. Ise
ATTN: TIO

Grumman Aerosp. Corp.
ATTN: J. Rogers, 533, Pt 35
ATTN: Tech. Lib.

GTE Sylv.
ATTN: Tech. Lib.

Hazeltine Corp.
ATTN: M. Waite, TL
ATTN: J. Colombo

Honeywell GAPD
ATTN: Tech. Lib.
ATTN: R. Johnson, A-1391

Honeywell RC
ATTN: Tech. Lib.

Hughes Acft.
GSGp
ATTN: Lib., 600, C-222

IITRI
ATTN: I. Mindel
ATTN: J. Bridges
ATTN: Tech. Lib.

Hughes Acft.
ATTN: K. Walker, D-157
ATTN: B. Campbell, 6-E110
ATTN: W. McDowell, R&D
ATTN: Dr. Binder, 6-D147
ATTN: Dr. Singletary, D-157
ATTN: Tech. Lib.

ITT
ATTN: Tech. Lib.

ITT
ATTN: D. Shaff

Litton Sys.
ATTN: F. McCarthy

LTV Aerosp.
ATTN: TDC

LTV Aerosp.
ATTN: T. Rozelle
ATTN: Tech. Lib.

MM Aerosp.
ATTN: Tech. Lib.

DISTRIBUTION LIST (Continued)

McDon. Doug.
ATTN: Dr. Ender, 313, 33
ATTN: Tech. Lib.

McDon. Doug.
ATTN: T. Lundregan

MRC
ATTN: Dr. Van Lint

Mitre Corp.
ATTN: Tech. Lib.

Northrop Elc. Div.
ATTN: Tech. Lib.

Northrop Elc. Div.
ATTN: Tech. Lib.

Philco-Ford, WDLD
ATTN: Tech. Lib.

Pulsar Asso.
ATTN: C. Jones

Rand Corp.
ATTN: Tech. Lib.

IITRI, ECAC
ATTN: Tech. Lib.

IRT
ATTN: Tech. Lib.

IBM
ATTN: Tech. Lib.

Ion Phys.
ATTN: Tech. Lib.

Kaman Sci.
ATTN: Tech. Lib.

Litton Sys.
Data Sys.
ATTN: S. Sternbach
ATTN: Tech. Lib.

Lockheed M/S
ATTN: TIC, G. Evans, O-52-52

MIT, Linc. Lab.
ATTN: A. Stanley
ATTN: L. Loughlin, Lib.

MM Corp.
ATTN: Tech. Lib.

McDon. Doug.
ATTN: Tech. Lib.

MRC
ATTN: Tech. Lib.

MRC
ATTN: J. Hill
ATTN: D. Merewether
ATTN: Tech. Lib.

NAS
ATTN: Dr. Shane, Nat. Mtls. Adv. Bd.
ATTN: Tech. Lib.

Northrop R&TC
ATTN: Tech. Lib.

Philco-Ford, A&COps.
ATTN: Tech. Lib.

Phys. Int.
ATTN: Tech. Lib.
ATTN: I. Smith

R&D Assoc.
ATTN: Tech. Lib.

Raytheon
ATTN: Tech. Lib.

Raytheon
ATTN: G. Joshi, Rad. Sys. Lab.
ATTN: Tech. Lib.

RCA, G&S Sys.
ATTN: Dr. Brucker
ATTN: Tech. Lib.

Rockwell Int.
ATTN: G. Messenger, FB-61
ATTN: R. Hubbs, FB-46
ATTN: J. Bell, HA-10
ATTN: J. Sexton, CA-31
ATTN: Tech. Lib.

Sperry Rand Gyro Mgt. Div.
ATTN: Tech. Lib.

Sperry Rand Univac Def. Sys.
ATTN: Tech. Lib.

Texas Instru.
ATTN: Tech. Lib.

BDM
ATTN: Dr. Neighbors

TRW Sys. Gp.
ATTN: A. Liebschutz, R1-2154
ATTN: J. Lubell
ATTN: A. Narevsky, R1-2144
ATTN: R. Whitmer
ATTN: R. Kingsland, R1-2154
ATTN: R. Webb, R1-1071
ATTN: F. Holmquist, R1-1070
ATTN: Dr. Sussholtz
ATTN: TIC, S-1930
ATTN: Dr. Jortner
ATTN: W. Robinette

UAC Ham Std.
ATTN: R. Gignere
ATTN: Tech. Lib.

Westinghouse D&ESC
ATTN: H. Kalapaca, 3525
ATTN: Tech. Lib.

Cdr.
USAR&DCtr.
ATTN: AMXRD-BVL, J. McNeilly
ATTN: Tech. Lib.

Cdr.
USASA
ATTN: IARD-T, Dr. Burkhardt
ATTN: Tech. Lib.

Litton Sys., G&CSD
ATTN: Tech. Lib.

RCA, G&C Sys.
M&S Rad.
ATTN: Tech. Lib.

RTI
ATTN: Dr. M. Simons, Eng. Div.

Rockwell Int.
ATTN: Tech. Lib.

Sci. Appl.
ATTN: Tech. Lib.

Sperry Rand Flt. Sys. Div.
ATTN: Tech. Lib.
ATTN: D. Schow, 104C

SRI
ATTN: Tech. Lib.

SRI
ATTN: Tech. Lib.

Texas Tech. Univ.
ATTN: T. Simpson
ATTN: Tech. Lib.

TRW Semicond.
ATTN: R. Clarke, Tech. Stf.
ATTN: Tech. Lib.

TRW Sys. Gp.
ATTN: Tech. Lib.

TRW Sys. Gp.
ATTN: D. Pubsley
ATTN: Tech. Lib.

UAC Norden
ATTN: C. Corda

Univ. Denver, CO Sem., DRI
ATTN: Tech. Lib.

Cdr.
USAADC
ATTN: Tech. Lib.

Cdr.
USAMC
ATTN: A. Nichols, NDB 300, 95
ATTN: Tech. Lib.

Ch.
NR
Dept. of the Navy
ATTN: R. Joiner, 464
ATTN: Tech. Lib.

CO
Diamond Lab.
ATTN: Lib.

HQ USAF
ATTN: XOOWD

AFSC
ATTN: DLCAW
ATTN: XRP

USAFA
ATTN: FJSRL, CC

AFIT
ATTN: Tech. Lib., 640, B

CO
USAEC
ATTN: AMSEL-10-T
ATTN: Tech. Lib.

DISTRIBUTION LIST (Continued)

Dir.
Ofc., LLL
ATTN: TID

HQ USAF
ATTN: RDQPN, 1D425

Dir.
BMD Prog. Off.
ATTN: Tech. Lib.

Westinghouse Elec. Corp.
ATTN: R. E. Wootton, 301-2B3

Auburn Univ., Physics Dept.
ATTN: Dr. P. P. Budenstein

Dir.
Ofc., LLL
ATTN: Dr. L. C. Martin, L-156
ATTN: Dr. J. Candy, L-156

State Univ. of NY at Buffalo
ATTN: Dr. J. J. Whalen

U.S. Army Msl. Comd.
2 cy ATTN: D. Mathews, DRSMI-RGP

Clarkson College of Tech.
ATTN: Henry Domingos

Hq USAF
AFTAC

ADC
ATTN: DPQY

AUL
ATTN: LDE

AFWL
ATTN: HO, Dr. Minge
ATTN: EL, J. Darrah
ATTN: ELA, L. Eichwald
ATTN: ELA, J. O'Donnel
ATTN: ELA, R. Hays
ATTN: ELA, D. Lawry
ATTN: ELA, Maj Nielsen
2 cy ATTN: SUL
15 cy ATTN: DYX, Dr. Wunsch

Lockheed M/S Co.
ATTN: Tech. Lib.

Official Record Copy, Maj Nielsen, AFWL/ELA